Design of Ultrasonic Processing Device for Aluminum Surfaces

by

Mohamed Mahmoud Yassin

A thesis
presented to the University of Waterloo
in fulfilment of the
thesis requirement for the degree of
Master of Applied Science
in
Mechanical Engineering

Waterloo, Ontario, Canada, 2018

Author's Declaration

This thesis consists of material all of which I authored or co-authored: see Statement of Contributions included below. This is a true copy of the thesis, including any required final revisions, as accepted by my examiners.

I understand that my thesis may be made electronically available to the public.

<u>Statement of Contributions</u>

I would like to acknowledge the names of my supervisor and colleague who contributed to the research presented in this dissertation:

- Professor Hyock Ju Kwon
- Yanjun Qian (PhD Student)

Abstract

The work in this thesis examines the design possibility of a device capable of harnessing ultrasonic oscillations through resonance such that it can be applied onto an aluminum surface to produce a compressive residual stress field. Particularly to solve the common industry issue of fatigue life failures around stress concentration areas such as holes and shape discontinuities. Purchase of a pre-assembled ultrasonic transducer was used to simplify the project, however the design research focuses on developing a Sonotrode or Horn capable of amplifying and focusing ultrasonic oscillations onto a sample surface. The development includes iterative analytical, numerical, and experimental design to achieve the final result. MatLab and Comsol software were used for analytical and numerical simulation models. Three iterations of physical designs were conducted including full steel body, combined aluminum and steel, and aluminum and carbide material design methods. The first two iterations were unsuccessful in achieving resonance due to incorrect design assumptions which lead to a mismatch in frequency resonance and a significant increase in system electrical impedance due to mass. The third iteration used a complete aluminum body with multi-stepped shape design and an attached carbide insert for tip hardness. A 200W precision ultrasonic driver and analyzer device made by Piezo Drive combined with a Laser Doppler Vibrometer was used for monitoring electrical and mechanical system response during operation. The result of this study shows that after true system resonance is achieved, maximum tip displacement occurs at the same frequency, and can be increased by increasing applied input voltage to the transducer.

<u>Acknowledgements</u>

Table of Contents

List of Figures

List of Tables

1.0 Introduction

Fatigue life failure of materials has become a big concern in various industries and has been reported as the majority of failures in the automotive industry. The surface properties of mechanical components and parts play an important role in fatigue life failures. The fatigue life of a specific component can be improved by using various surface treatment methods. Many of the currently available methods cannot meet the time and resource constraints of practical industry [1,2]. However, one of these methods is ultrasonic surface treatment (UST) which harnesses the resonance phenomenon thus producing large amplitude of oscillations which are applied to the specimen surface [3]. The vibration energy is channeled onto the surface using a tool and impacts with thousands of strikes in a short period of time. Since the resonant frequency is in the ultrasonic range (~20 kHz), this method can be used to alter the surface in a fast and controlled manner. These strikes create a plastic deformation of the surface in the form of micro-dimples which lead to the material becoming cold-forged, thus improving the mechanical fatigue properties. Similar methods of surface hardening have been demonstrated to substantially improve the mechanical fatigue and wear properties of a material through compressive residual stress [1,2,4].

Piezoelectric plates can be used to create an ultrasonic transducer traditionally referred to as a Langevin transducer which is able to achieve the ultrasonic oscillations required to excite the focusing tool (horn) in a longitudinal manner to strike the surface of the metallic sample under processing. Research is scarce on developing these ultrasonic transducers for the application of UST surface processing; however, similar devices do exist that have similarities to dedicated UST devices. Some of these other devices can be used in replacement, which can be found in industry used as tools for welding, cutting, or drilling [3,5].

The developmental design of an ultrasonic transducer for this exact application requires extensive research and resources, purchase of a prefabricated ultrasonic transducers was suggested by the supervising professor of this project for overall simplicity. Based on the target frequency of 20 kHz ultrasonic transducers used for welding applications are the closest available. The transducer is discussed later in the procedure and setup section, however a welding transducer was purchased from Honda Electronics (Aichi, Japan), which is designed to operate at the target frequency of 20 kHz for use in this research project.

The objective remaining is to design a booster horn tool which can amplify the longitudinal oscillations and condense the strike force into a small tip. This horn, sometimes referred to as a sonotrode should be designed to have a natural frequency (Eigen-frequency) matching the output frequency of the transducer previously acquired such that true resonance is achieved [2,3,4]. The Eigen-frequency of the horn can be approximately calculated and adjusted before manufacturing using finite element analysis (FEA) software such as COMSOL. The decreasing size shape towards the tip end creates an amplification or focusing action of vibrations for increased force per area of contact, thus the horn should start with a large diameter and end with a smaller diameter of desired amplification ratio. There are several different shapes which can be used to design the horn, some commonly used shapes are tapered (conical), exponential, and stepped. Each of the shapes has a unique shape function along the length which they are defined, however these details are discussed in the design section of this report.

1.1 Background Information

Ultrasonic Waves

The definition of ultrasonic is a sound wave which is "of or involving sounds waves with a frequency above the upper limit of human hearing" [6]. The acoustic range or maximum human hearing range is approximately between 20 Hz and 20 kHz, while the average adult may lose a small amount of hearing from the ends of the spectrum over time (caused by aging) or due to damage from other sources such as exposure or illness [6]. The lower end of the spectrum which is below 20 Hz is referred to as infrasound and has other application uses, both natural and artificial. Some technology, equipment, and natural creatures can take advantage of this ultrasound frequency range for a variety of applications. The table below (table 1) shows some examples and breakdown of the sound wave ranges.

Table 1: Detailed description of Various Sound Wave Types [7,8,9,10]

Sound Wave type	Infrasound	Acoustic	Ultrasound	High-end Ultra
Range	< 20 Hz	20 Hz - 20kHz	> 20 kHz	>100 kHz
Application	Long distance communication	Short distance communcation	Power application	Detection and Navigation
Natural	Whales, elephants, and earthquakes	Humans and most animals	Bats, insects, dogs	Low power ultrasonics
Artificial	Monitoring of Earthquakes and weather patterns	Communications and some science applications	High power ultrasonics	Medical diagonstic applications

Vibration Modes

Generating a small vibrational wave can be achieved by applying an electrical pulse of current onto a piezoelectric element. A Langevin transducer or sandwich transducer is capable of wave propagation by squeezing piezoelectric elements between two masses on the front and back sides of the elements. However, to amplify this small vibration into a useful ultrasonic application requires more components. Research on the development of ultrasonic transducers is readily available and multiple sources validate the use of the sandwich structure and the requirements of pre-stressing, however in this project a preassembled transducer was purchased directly to simplify the system and focus resources on development of the focusing horn tool [2,4,5].

There are 3 main modes of vibration which can be harnessed based on the design parameters of the transducer system [2]:

Longitudinal - *forward and aft motion*
Torsional – *twisting/radial motion*
Flexural - *bending motion*

Combinations of these modes are also possible [3], however the longitudinal mode is the only vibration mode required for the application of UST since the strikes are similar to a vertical hammering motion. The focusing horn tool (sonotrode) is a separate component from the transducer assembly and has its own set of natural vibration frequencies referred to as Eigen-frequencies, at which it resonates. Therefore, the horn tool should be designed to have the longitudinal mode Eigen-frequency match the driving frequency provided by the transducer. Examples of different vibration modes achieved for the same part at a wide range of frequencies are shown below (Figure 1).
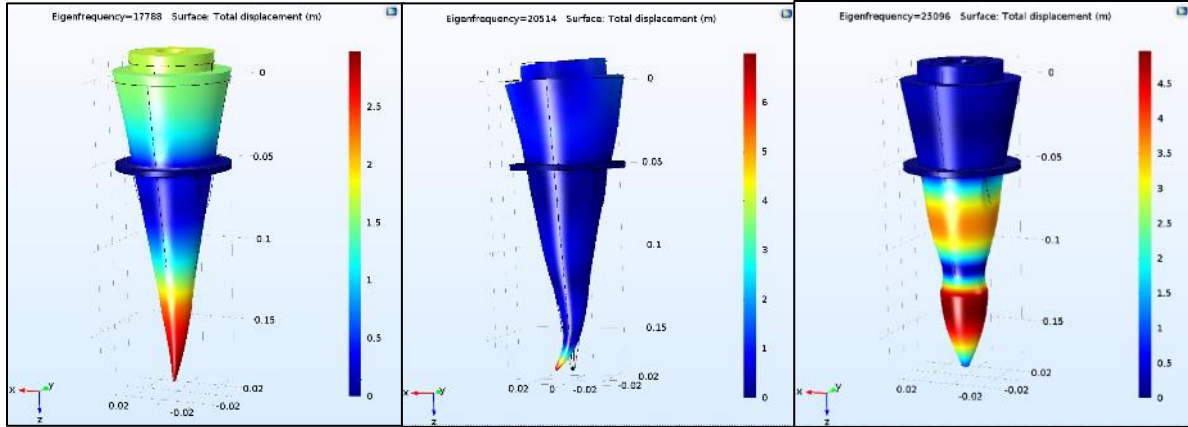
Figure 1: Different eigen frequency vibration modes of the same horn. Longitudinal at 17.8 kHz (left), Flexural at 20.5 kHz (middle), Radial at 25.1 kHz (left)

Compressive Residual Stress

Fatigue life failure occurs when a material is subjected to repeatedly applied loads and a localized crack appears then grows into final failure. Failures of this type can be difficult to predict accurately, however the life of materials can be increased or decreased by numerous influencing factors such as residual surface stress and transition geometry. Assuming that a part should be designed to have a specific geometry and the determined current fatigue life is a fixed number of cycles, it is possible to increase this cyclic life by applying compressive residual stress (CRS) to the surface [5,11].

The cyclic loading stresses are greatest at the surface of a metal, thus crack initiation will usually occur there. Introducing a compressive residual stress field on the surface of the metal by applying plastic deformation reduces the magnitude of tensile stress at the surface [11]. Crack initiation therefore is driven down below the surface where cyclic stresses may be lower than maximum leading to an increase in overall fatigue life [12,13].

Most current industry application of CRS is through shot peening, which includes blasting the surface with a media of small metal ball bearings or hardened sand. If UST is able to create the same CRS effect it can be used to create surface patterning effect similar to plastic deformation, however in a much more efficient and versatile manner. [1,4]

1.2 Previous Literature

Many articles have previously noted the improvement of cyclic fatigue life through surface property changing methods such as shot peening. This is mostly due to the phenomenon referred to as compress residual stress as discussed in the previous section. Controlled shot peening is a cold surface treatment widely used in automotive and aerospace industries. Generally, shot peening is an effective method for improving the fatigue behavior of mechanical components. The beneficial effects of this process are attributed to the Compressive Residual Stresses (CRS) fields and the surface work hardening [11,13,15,16].

Shot peening (SP) has been one of the most widely used methods historically however, this study points out that the inconsistent manner of processing with a media such as 'shots' leads to an inconsistent treatment across the surface of the specimens [14]. Shot peening process is a cold-based treating method for modifying material surface upon which surface micro-cracks or tensile residual stresses exist. SP is commonly used for aircraft repair, gear parts, turbine components, connecting rods, etc. During SP, specimen surface is bombarded by small spherical shots in a randomly impacting fashion. The thickness and material behavior of the treated layer is not homogenous throughout the surface under this treatment. [14]

In the late 1950's another method of surface peening began to arise referred to as ultrasonic peening treatment (UPT), however it wasn't until much more recently that complete applications of it were used. One article describes the original technique as generating continuous ultrasonic vibrations at a carburized steel (hardened) tool tip, the treated part surface received direct impacts. [15]

Most of the previous applications used UPT to improve fatigue life around welds to counteract heat affected zone weaknesses. Harmful tensile residual stresses are effectively eliminated and a layer of compressive residual stresses is exerted to the metal surface. The UPT process is therefore able to increase surface micro-hardness, corrosion resistance, and enhances fatigue life and strength [17].

Multiple papers mention that there can be significant limitations to using ultrasonic vibration for surface treatment, which prevent the wide usage of these methods in ultrasonic applications. These limitations are the complex design and excitation, possible coupling with surrounding modes, instability in operating at different boundaries, difficulty in securing the structure without influencing the vibrational response [18,19].

However, a more recent review article shows that improvements in technology may allow ultrasonic treatment methods to become a more viable option and further research is required to develop it. "Ultrasonic peening treatment (UPT) is one of the most promising methods in the cold treatment of metallic materials" [15]

1.3 Project Objective

The main objective of this project is to develop a single novel device which is capable of producing ultrasonic surface treatment allowing a way to explore the technology in a more mass-production setting. A UST device will typically have 4 main components: the high frequency power source, the piezoelectric transducer, the booster (frequency amplifier), and the sonotrode or horn (focusing tool). The transducer's role is to convert electrical input into high frequency mechanical energy (in the form of vibrations). The booster modifies the amplitude of the vibrations coming from the conversion, while the horn fine tunes the amplitude and applies it to the surface of the test specimen.

For simplification of this project the booster and horn may be combined into a single sonotrode tool (horn) capable of amplifying and focusing the vibrations simultaneously, and a Langevin type transducer was purchased previously assembled from an industry supplier. Creating a sonotrode for this exact application requires extensive finite element analysis (FEA) modeling such that the resonance frequency can be matched correctly and amplitude of ultrasonic waves is maximized. It also requires relatively precise manufacturing and assembly of the completed device, including proper fixture environment to house the device without altering the resonance while applying the ultrasonic oscillations onto test specimens. The UST needs to be applied onto a surface rather than a single point, therefore, purchase and use of a multi-axis computer numerically controlled (CNC) device is advantageous.

The objectives will be achieved in the form of detailed calculations, iterative experiments, proof-of-concept designs, and this encompassing research report. The recommendations on continued research and future development are also important outputs of this project. In short, this research attempts to address the question whether it is possible to develop an ultrasonic processing device which is capable of producing compressive residual stress field on the surface of an aluminum sample.

2.0 Horn Design

Horn design was broken down into three sections, shape design, analytical design, and iterative numerical simulation. The device geometry and profile of the horn is detailed in shape design section (2.1). The mathematical calculations derived by Yanjun Qian (PhD Student Colleague in Research Group) are explained and lead to MatLab code results of section 2.2. Finite element models of the device resonance are discussed in the iterative numerical simulation section (2.3)

2.1 Shape Design

The role of the sonotrode or horn is to boost or amplify the mechanical oscillations while also applying them to the surface of the sample part being processed. There are several different types or shapes of ultrasonic horns which can be used to achieve various results, each having their own benefits and drawbacks. Shown below (Figure 2) are 3 common shape forms which will be considered: Stepped, Conical, and Exponential [3,5,18].
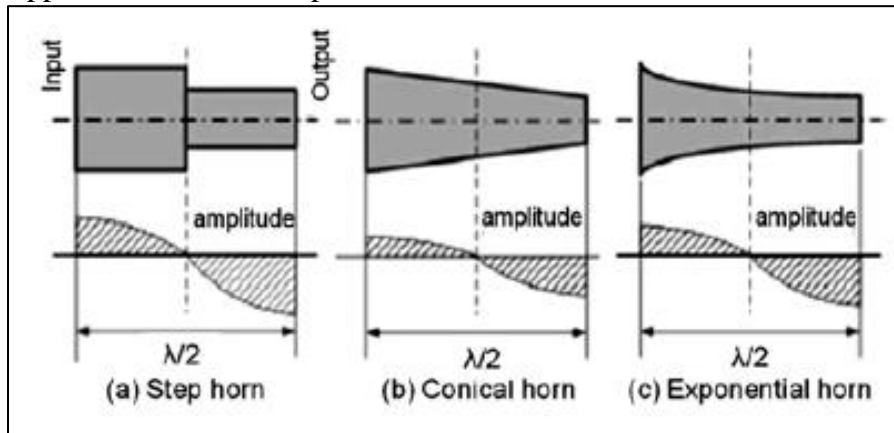
Figure 2: Basic shape designs of half wavelength horns showing input to output end [3]

Shape A is referred to as stepped horn, and is by far the simplest design and physical manufacturing requires little effort [2,3]. However the drawbacks are that the stepping section should only occur at precisely the nodal section for practical fixture reasons and there are limitations that come with amplification ratio and overall length of the thinned section becoming impractical [5]. Shape B is conical or linear tapered, and it adds some level of complexity to manufacturing however a skilled machinist with the sufficiently capable equipment such as a computerized motion lathe would be able create this. With a conical shape the nodal section ring can be simply moved throughout the structure without significantly affecting the overall design. Shape C is referred to as exponential due to its similarity in profile to exponential curves. This shape typically provides the best resultant increase in amplification without any major discontinuities, however from a physical manufacturing standpoint it becomes very difficult to machine precisely even with the aid of computerized machining and simulation may differ from the actual result leading to significant error in outputs [3].

A combination of multiple shapes could also be possible [2]; examples of such designs may incorporate advantages from each basic shape and are shown below (Figure 3). These design examples are influenced by sprinting spike shoes in athletics. The pin shapes are used in running shoes to increase force per contact area which allows the runners to maintain friction when applying large force to the ground. Similarly the focusing effect of load can be directly applied to

UST and thus these multi shape designs could help in simplifying manfacturing process of repeated horns.
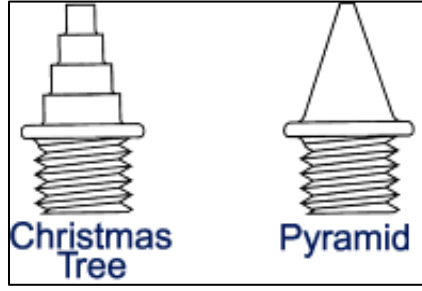
Figure 3: Image of running spike pins used to demonstrate multi-shape design examples

Similarly one can use a combination of a simple shape function such as stepped with multiple segments to approximate or simulate a more difficult to manufacture design; noting that the size of the steps determines the accuracy compared to the more complicated to manufacture original curved shape (see Figure 4 below).
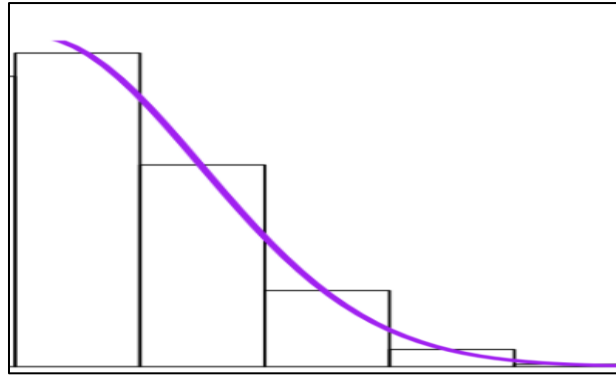
Figure 4: Image showing the comparison between a curved shape and multi-stepped design

These shapes are be represented in analytical form by shape functions of the radius over the entire length; see the following table (Table 2) taking from articles on design of ultrasonic machining tools [5,18]. Further discussion on the use of these shape functions is included in the following section as part of analytical design.

Table 2: Various horn shape designs with their corresponding shape parameters and functions [18]

SONOTRODE SHAPE		SLENDERNESS RATIO	SHAPE PARAMETERS	SHAPE FUNCTION
cylindrical			$-$	$r(x) = r = \frac{d_0}{2}$
tapered			$\alpha \in \langle -5°; 5° \rangle$	$r(x) = \frac{d_0}{2}(1 + l_0 \tan(\alpha))$
exponential		$\delta = \frac{d_0}{l_0}$	$a \in \langle 0.3; e \rangle$	$r(x) = \frac{d_0}{2} a^x$
stepped			$\eta = \frac{l}{l_0}$ $\eta = \{0.25; 0.5; 0.75\}$	$r\{x \in \langle 0; l \rangle\} = \frac{d_0}{2}$ $r\{x \in (l; l_0)\} = \frac{d}{2}$

7

2.2 Analytical Design

Design of the horn geometry requires extensive analytical calculations, as there are several parameters which will affect the final resultant natural frequency (Eigen-frequency) of the horn. The first parameter to consider is the material of the horn which the waves are propagating; in this case it is a solid metal for practical application reasons. Sounds waves can travel through multiple different media including gases, liquids, and solids. As previously discussed in section 1.1, ultrasonic waves are a form of sound waves in the ultrasonic range (>20 kHz frequency) and relating to UST these waves are travelling through a solid media. Determining the propagation speed of these waves in a particular media is predicted by the relationship between elastic properties and density of the media. The elastic property of metal referred to as young's modulus (E) is used to determine the wave speed within the sonotrode. The following formula represents this relationship and an example of steel is shown below [19]:

$$c = \sqrt{\frac{E}{\rho}} \tag{2.1}$$

where:
c is the sound wave velocity (m/s)
E is the modulus of elasticity (N/m^2 or Pa) [20]
ρ is the density of the material (kg/m^3) [20]

$$c_{steel} = \sqrt{\frac{E_{steel}}{\rho_{steel}}} = \sqrt{\frac{210 \times 10^9 \ (N/m^2)}{7900 \ (kg/m^3)}} \cong 5156 \ (m/s)$$

Discussed in the previous section (2.1 Shape Design) are some of the different possible shape functions to create a typical horn. Since most of this research uses a conical shape approach the sample calculations below are to determine the parameters of the device. The two important parameters to be determined are overall length, nodal point (x_{node}) along the length of horn. The initial radius of the horn is determined by the transducer specifications, while the tip end radius is set by the user requirements and application.

Starting with the conical geometry shape function over the entire length where $0 < x < L$ and the decreasing slope angle(α); the radius of the cone at each x location can be determined as follows [18]:

$$R = R_1(1 - \alpha x)$$
$$S = S_1(1 - \alpha x)^2 \tag{2.2}$$

where α can be expressed as:

$$\alpha = \frac{R_1 - R_2}{R_1 L} = \frac{1}{L}\left(1 - \frac{1}{N}\right) \tag{2.3}$$

Note:
R$_1$ is the initial radius (transducer end)
R$_2$ is the final radius (tip end)
N is the amplification ratio (R$_1$/R$_2$)

It is known that:

$$K = \sqrt{k^2 - \frac{1}{\sqrt{S}}\frac{\partial^2 \sqrt{S}}{\partial x^2}} \rightarrow K = k \qquad (2.4)$$

where:

Wave number variable $k = \frac{\omega}{c}$

Equivalent wave number K

Frequency $f = \frac{\omega}{2\pi}$

This leads to the displacement distribution function (ξ) as [3,21]:

$$\xi = \frac{1}{\sqrt{S}}(A\,cosKx + B\,sinKx) \qquad (2.5)$$

Although square root of S is what was derived previously, if the constant is factored out and compensate it with alternate A and B, x related term will become easier to differentiate without additional constant multiplier. The nodal point (x $_{node}$) occurs where the displacement is zero and L will be at the end where velocity (derivative of displacement) is zero. Therefore, differentiating to solve for these as follows:

$$\xi = \frac{1}{x - \frac{1}{\alpha}}(A\,cosKx + B\,sinKx) \qquad (2.6)$$

$$\frac{\partial \xi}{\partial x} = -\frac{1}{\left(x - \frac{1}{\alpha}\right)^2}(A\,cosKx + B\,sinKx) + \frac{K}{x - \frac{1}{\alpha}}(-A\,sinKx + B\,cosKx) \qquad (2.7)$$

$$\left.\frac{\partial y}{\partial x}\right|_{x=0} = \left.\frac{\partial y}{\partial x}\right|_{x=l} = 0 \qquad (2.8)$$

$$A = -\frac{k}{a}B \qquad (2.9)$$

$$tan\,kx = \frac{kL}{1 + \frac{k^2}{\alpha^2}(1 - \alpha L)} \qquad (2.10)$$

$$\alpha = \frac{N-1}{N}\frac{1}{L} \qquad (2.11)$$

$$tan\,kL = \frac{kL}{1 + \frac{N(kL)^2}{(N-1)^2}} \qquad (2.12)$$

$$L = \frac{kL}{K} = \frac{c}{2\pi f}kL \qquad (2.13)$$

9

$$\xi|_{x=0} = \xi_1 \text{ and } \xi|_{x=l} = \xi_2 \text{ and } \left.\frac{\partial \xi}{\partial x}\right|_{x=0} = 0 \tag{2.14}$$

$$A = -\frac{\xi_1}{\alpha} \text{ and } B = \frac{\xi_1}{k} \tag{2.15a/2.15b}$$

$$\xi = \frac{1}{x - \frac{1}{\alpha}}\left(-\frac{\xi_1}{\alpha}\cos kx + \frac{\xi_1}{k}\sin kx\right) = 0 \tag{2.16}$$

$$\tan kx_{node} = \frac{k}{\alpha} \tag{2.17}$$

$$x_{node} = \frac{\arctan\left(\frac{k}{\alpha}\right) + n\pi}{k} \tag{2.18}$$

Also determined was information about strain distribution and the maximum strain location, these calculations are shown in appendix A. Finally, these functions can be plotted on software such as MatLab to produce a two dimensional (2D) image of the approximate calculations. The MatLab code is attached in appendix B and an example output plot of the code is shown in the figure below (Figure 5):
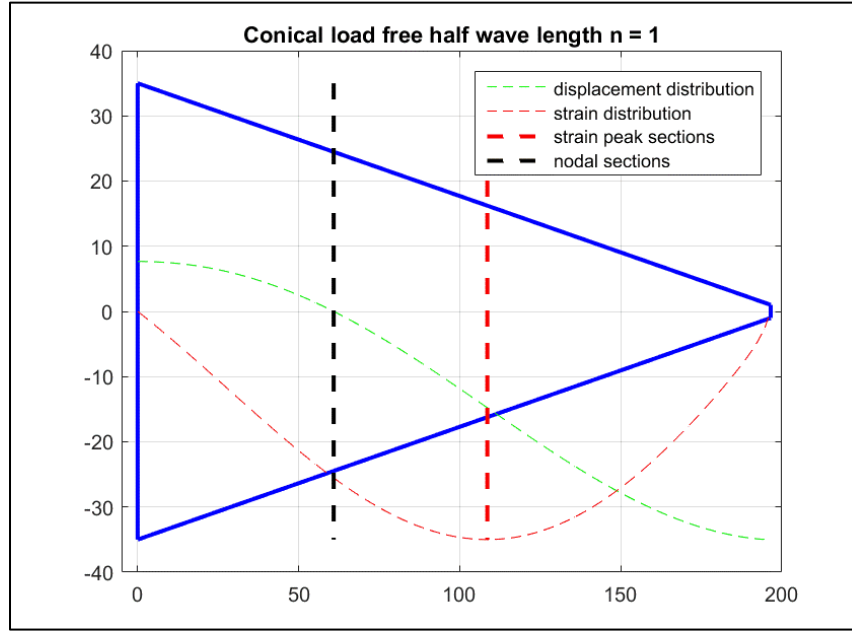
Figure 5: Example output plot of MatLab model used to calculate parameters of cone shape (Aluminum, 18 kHz target, 75 mm input, 1 mm output)

Note: The blue line shows the rough geometry outline and all dimensions shown are in millimeter (mm).

This resulting plot was rotated about the center axis to be used as a simple guideline for creation of the solid three-dimensional (3D) model of a horn with a half wave length and conical shape. The nodal section in this modal is a single point plane of infinitesimal thickness, therefore placement and dimensions of a gripping flange with reasonable thickness requires another

approximation to be determined by each user. In some cases, it may be easier to have the true nodal point be on one end of the nodal flange rather than in the center of the thickness; this depends on the experimental fixture design discussed in another section of the report (section 3.0).

2.3 Iterative Numerical Simulation

As previously discussed (section 1.1) the sonotrode (horn) should be designed to match the frequency of the transducer device and the intended longitudinal vibrational mode. To achieve multiple repetitive designs while attempting to match the frequencies, simulation using finite element analysis can be advantageous. For example, the overall shape of the device can be fixed as one conducts a parametric sweep of specific entities such as material or dimensions while setting the desired final frequency (20 kHz) as the goal. Setting realistic boundary and application conditions allows for an estimated simulation of numerous parameters or output results without having to physically manufacture multiple physical devices to be tested. COMSOL is a powerful finite element simulation analysis tool which is used for this repetitive testing to aid in development of the final sonotrode design.

Starting with the simplified 2D design which was analytically calculated using MatLab in the previous section and evolve into the product which will include practical values and geometries. Items such as adding threads for attachment, combination of materials, and true thickness of the nodal flange are all included in this iterative simulation. Each change in geometry directly affects the resonance of the part and fine tuning adjustments to the horn's main dimensions (length and slope) are required throughout the process.

Boundary conditions added into COMSOL to simulate some of the physical items which would be imposed onto the horns during processing. The first boundary condition was to set a fixed nodal flange, this simply was elected on the nodal flange ring surface. The second boundary condition was to simulate the added weight of the transducer on the top of the horn, approximated to be 1 kg or 9.8 N. For all models a tetrahedral mesh with a fine element size (maximum: 0.005 m /5 mm, minimum: 5E-4 m /0.5 mm) was selected to reduce the need for a mesh convergence study. Lastly, a mesh distribution was applied to refine the element size at the tip of the horn, since those areas are of main interest and have smaller geometric dimensions [22].

The first two horn iterations used a cone shape which were mostly modeled in MATLAB, directly revolved into a 3D model and then only refined slightly by the finite element analysis. However, the final design used in this report was multi-stepped and the following procedure methodology explains how it was developed numerically [22]. Beginning with parameters based on the previous calculations from MATLAB with inputs as:

- Input Diameter: 50 mm
- Output Diameter: 10 mm
- Target Frequency: 20 kHz

Out of simplicity a 4 step design method was chosen with diameter steps of 50 mm, 35 mm, 20 mm, and 10 mm. From iterations of previous designs it was known that the approximate length of the horn was 160 mm for a similar setup with conical shape. Applying the above mentioned items into COMSOL progresses into beginning a parametric sweep of each segment's length used to determine the correct overall length which achieves the target frequency. The flow chart explains each step of numerical iteration and the final design as simulated in the figures shown below (Figure 6, Figure 7). The flowchart excludes other iteration steps which were taken that lead to negative results, since those only apply for each particular cases of each research application.
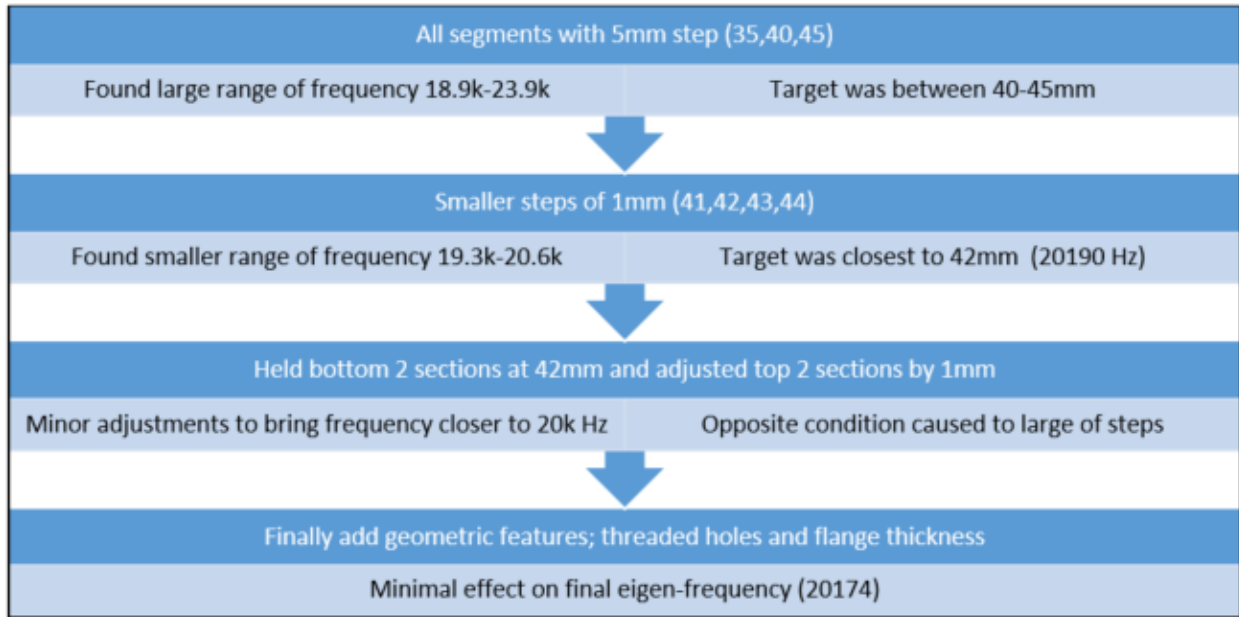
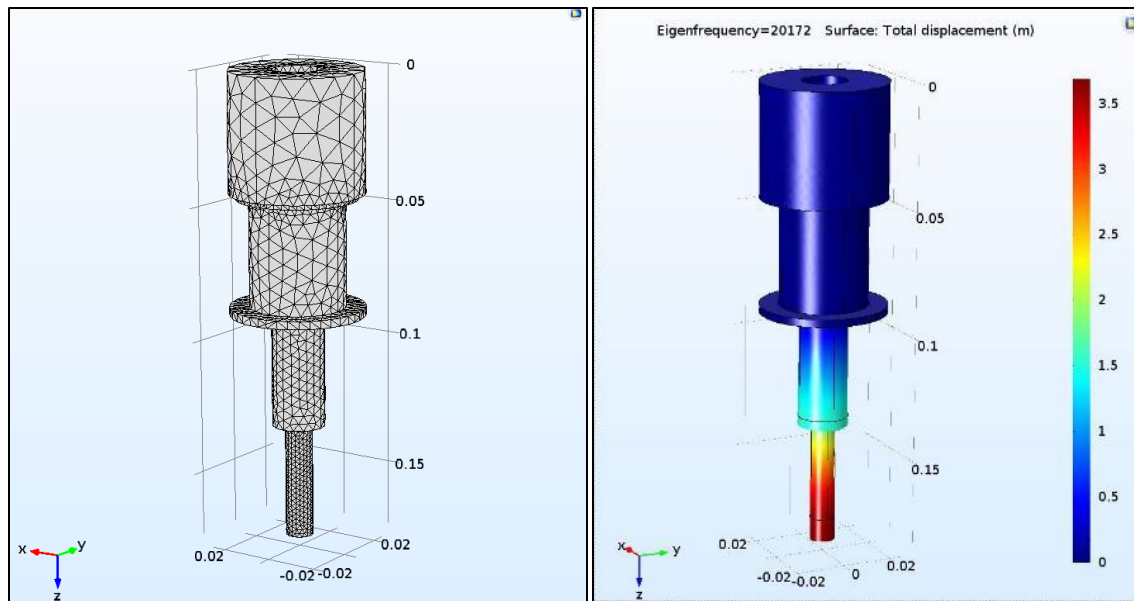*Figure 6: Flow chart of numerical iterations for multi-stepped horn design*

Figure 7: Multi-stepped horn design simulation in COMSOL, Mesh (Right), and Eigen-Frequency (Left)

3.0 Experimental Procedure and Setup

Nodal Flange Fixture

Physical contact or loads applied to the transducer and horn system may have an effect on the vibrations, therefore the best location for mounting the assembly is at the zero displacement plane [2,3]. As previously discussed (section 2.2) this zero displacement plane is called the nodal section, which is replaced by a nodal flange of a specified thickness (~3 mm). A clamping fixture/mechanism is to be designed such that it only contacts the horn assembly at the nodal flange. This fixture will then be moved as a whole through the 3-axis CNC machine. The fixture has a 2-piece design, with a pocket base and a covered piece bolted together. The base section created used a milled pocket of similar depth to the flange thickness and width dimension just slightly larger than the flange diameter. This allows for the flange section (ring) to be press fit inside the pocket and not move around during excitation. The top cover piece prevents the device from falling or moving vertically out of the pocket and allows for upside down mounting required when laser measuring vibrations which requires mounting vertically above the device (see physical results – laser testing section for more details).

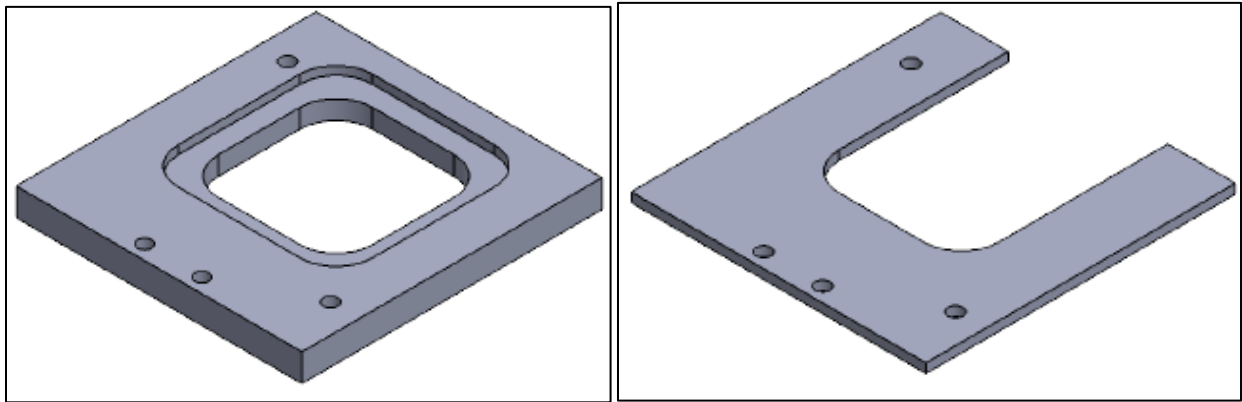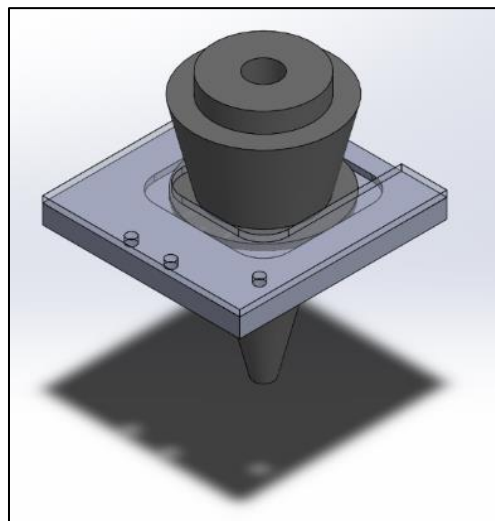*Figure 8: 2 piece fixture design. Base piece (Left), Top cover piece (Right)*

Figure 9: Assembled fixture with sample horn held inside, transparent cover shows pocket mating with nodal flange.

Free Z-Axis Motion

Purchase of a 3-axis CNC system was made to control the device, however only a 2-axis machine (i.e.: XY platform) was required for purpose of flat sample surface processing. Therefore,

nullification of the 3rd (Z) axis becomes a requirement of the mechanism, since this degree of freedom is used to control the applied vertical (Z-direction) force. As the tool tip moves across a seemingly flat surface, it may encounter some surface roughness which directly affect the applied load. With a free vertical axis it is possible to take advantage of the device's weight under gravity load being the only applied vertical force. This concept is achieved by integrating a sliding rail mechanism into the clamping fixture, where the front (horn and transducer) may fall freely onto the sample (free Z axis) and the CNC machine section controls the remaining axis' (X and Y) motions. The previous figures (Figure 8, Figure 9) show preliminary CAD designs of the clamping fixture mechanism (Note: rail mechanism not shown in figures) which is used to mount the horn assembly to the CNC machine.

Tool Path CNC Programming

The goal of the project is to process a surface section of a flat specimen, however the tool tip has a small contact surface area with the specimen. Therefore, this requires repetitive movement of the device across the surface which is easily automated using a computer numerical control (CNC) machine. A simple square sinusoidal or 'snake' pattern is used to cover a larger rectangular surface (Figure 10 shown below). Incorporated into the feed rate of the device is rapid movement which occurs at each end of the path (indicated by red) and a slower movement used during processing segments (indicated by blue).
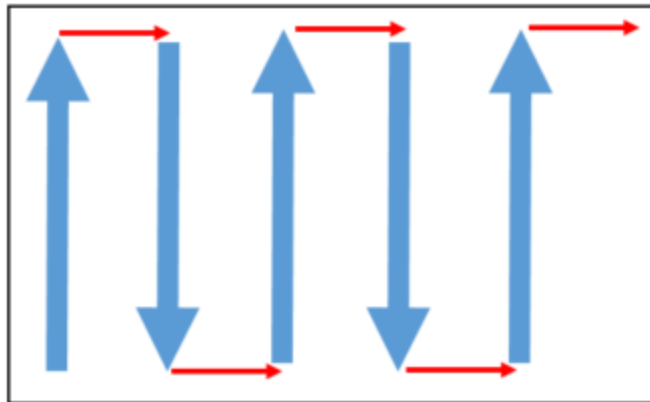

Figure 10: Square sinusoidal tool path pattern used to control device movement when attached to the CNC

The complete code for this setup is attached in Appendix C. It should be noted that the directional parameters used in the loops can be adjusted to accommodate any desired path size and tool tip width.

3.1 Manufacturing of Physical Prototypes

Once the horn designs were finalized numerically they were then sent out to a local machining center to manufacture them from steel (RJB Machining Ltd.) The goal is to process an aluminum surface, thus the horns required to be made from a harder material such as steel, this made machining using a small student machine shop difficult. Also due to the complexity of original horn design, a basic manual lathe would be insufficient and requires a CNC lathe to achieve the sloping cone shape. The figure below (Figure 11) shows a Solidworks part drawing of the design which were sent out to the machining center.
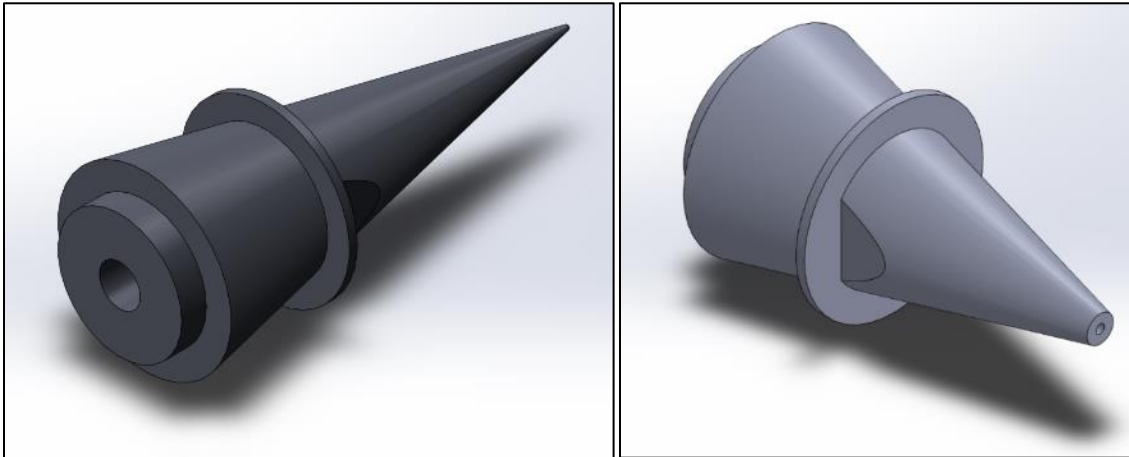

Figure 11: Solidworks rendering of 1st Prototype Full steel body (Left) and 2nd Prototype Aluminum Body without tip (Right)

In later iterations it was attempted to use aluminum rather than steel for the body of the horn and simply attach a hardened tool tip, discussion on the explanation is available in section 4.1. The overall shape design of these first 2 iterations did not differ greatly, simply the difference between them was dimensions and material which were calculated numerically using COMSOL as previously stated. The figure above shows solid works part drawing for each of these (Figure 11), note the overall length of the aluminum tool was smaller than the steel tool by approximately 30%. Photos of the physical prototypes are shown in the figure below (Figure 12).

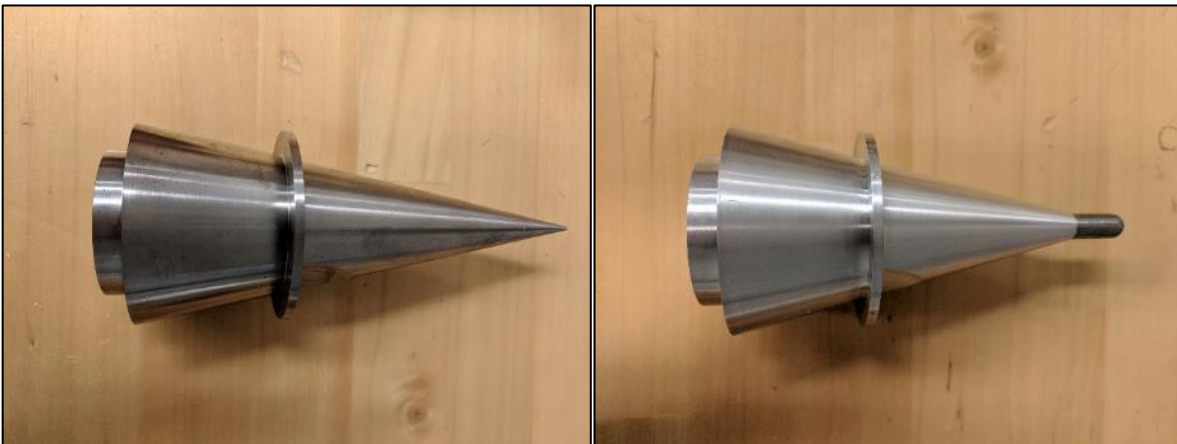*Figure 12: Physical picture of 1st Prototype Full steel body (Left) and 2nd Prototype Aluminum Body with steel tip (Right)*

The 3rd iteration prototype was also machined out of aluminum and incorporated a more simple to manufacture design. The design for this device was straight stepped with simple cylindrical segments allowing for cost savings of device machinability in the university's student

machine shop. Solidworks image and photo of the physical part are shown below (Figure 13), note that the machined surface quality and geometric tolerances of this prototype are slightly inferior (+/- 0.5 mm tolerance) than the previous professionally machined horns of 1st and 2nd iterations due to limited capability of the student machine shop tooling.
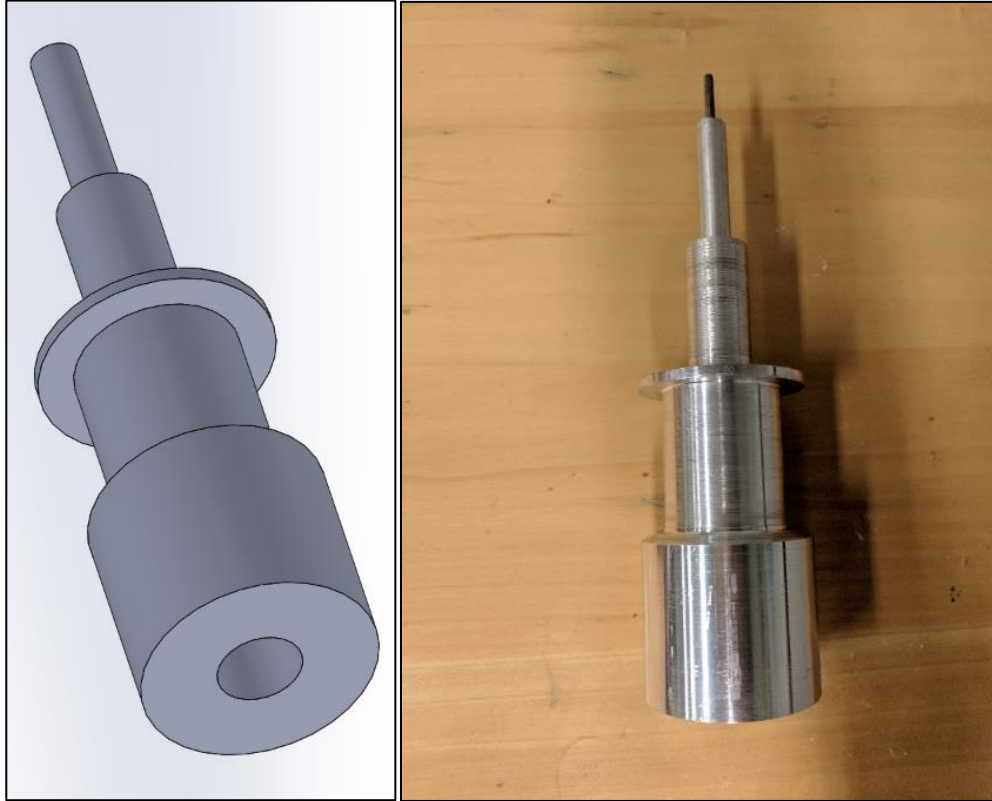

Figure 13: Images of multi-stepped horn Solidworks and physical part

3.2 Response Testing Equipment

Ultrasonic Driver and Analyzer

A 200W precision ultrasonic driver and analyzer device (PDUS200) made by PiezoDrive was purchased and is used to power the ultrasonic transducer in this system [23]. This device drives the piezo electric discs by generating a sinusoidal wave output of electrical power. There is a wide range of applications for this device such as ultrasonic drilling and cutting, medical devices, dental devices, ultrasonic testing, liquid cavitation, and vaporization [23]. It also features built-in resonance tracking, signal monitoring, power monitoring, and frequency response analysis of the transducer impedance through the desktop application and USB interface [23]. It was possible to adjust the settings of the device accurately and record most input and output conditions through this desktop application. A sample of the input screen during operation is shown in the figure below (Figure 14); note the top right plot shows the actuator voltage and current while the bottom plot shows the time history of the frequency and phase.
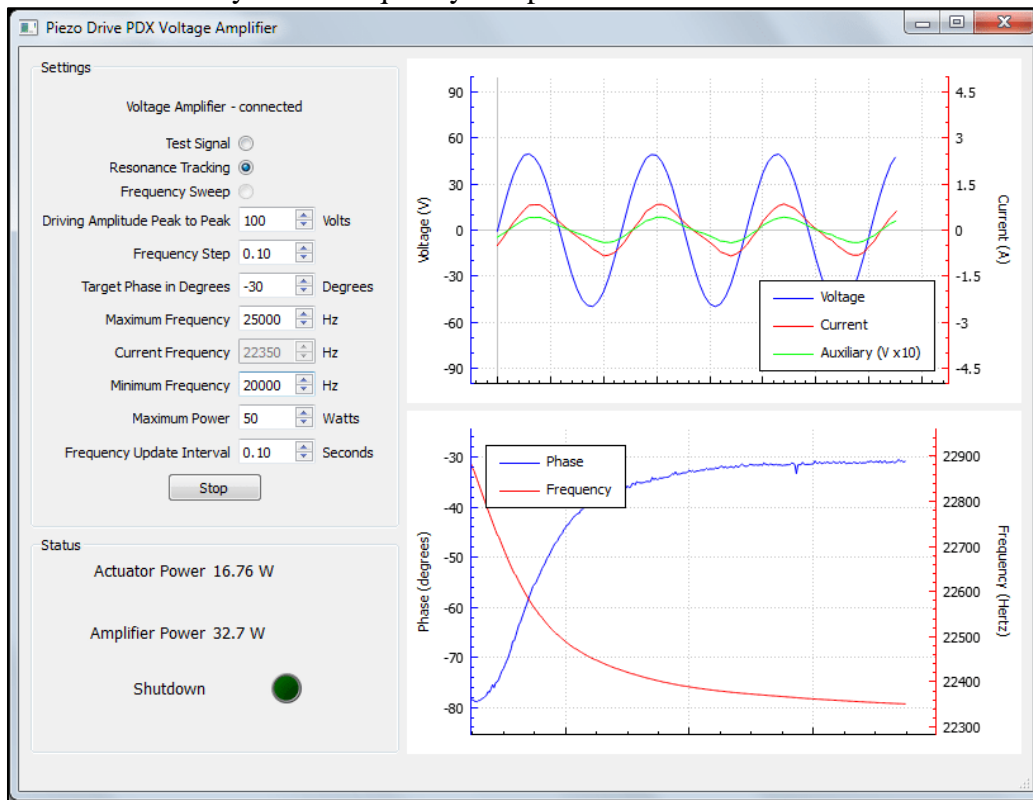

Figure 14: Sample Output of Piezo Drive software showing possible operation and input parameters

The main use of this device for this project is to characterize electrical and mechanical response of the system. The analyzer device is able to do this through the frequency sweep function which is intended specifically for transducer development and troubleshooting or monitoring industrial machinery. Essentially, the device drives the transducer system at a specified range of frequencies and outputs the resultant impedance magnitude and phase angle (electrical portion) and auxiliary signal transfer function (mechanical portion). Shown in the figure below (Figure 15) is an image of the output screen conducting a frequency sweep of the ultrasonic transducer used in this project without any attached horns.
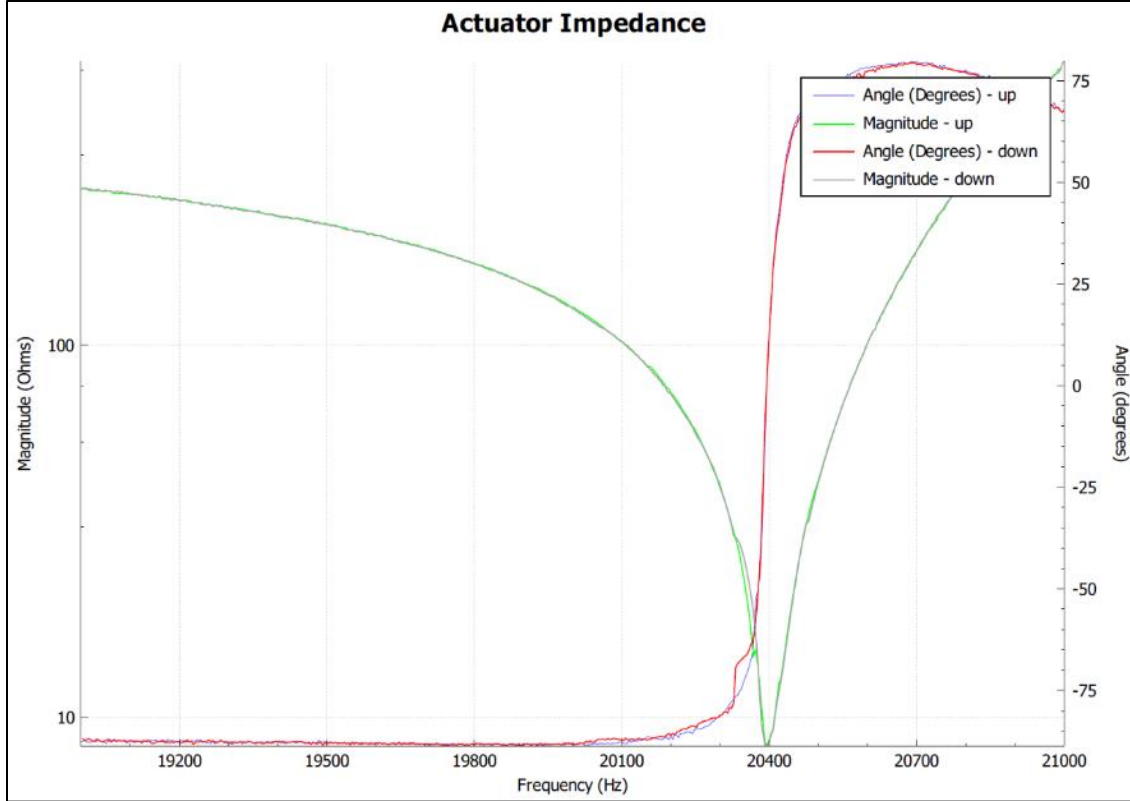
Figure 15: Plot of electrical impedance sweep taken of Honda transducer only

Note: that mechanical response auxiliary output was not being monitored and not shown here.

Based on this plot figure it was concluded that the resonance frequency of the transducer is approximately 20400 Hz since this is the location where magnitude of impedance is minimized and phase angle becomes zero degrees. Therefore the horn device should closely match this frequency to take advantage of resonance.

Electrical impedance is a measure of opposition of a circuit current when a voltage is applied. It is comprised of 2 imaginary and 1 real component: capacitance (C), inductance (L), and resistance (R). Together these three makes up the whole magnitude of electrical impedance (Z) defined as [24]:

$$Z = \sqrt{R^2 + (X_L - X_C)^2} \tag{3.1}$$

Capacitance and inductance are 180 degrees apart in phase and both perpendicular to the resistance. The system can have capacitive behavior (negative phase angle), inductive behavior (positive phase angle) and resonance (zero degree phase angle). This phase angle (φ) can be found using the vector calculation as follows:

$$\varphi = tan\left(\frac{X_L - X_C}{R}\right) \tag{3.2}$$

Discussion on the use of these values is available in the next section of the report (4.0 Resonance Frequency Matching: Electrical Response)

19

Laser Vibrometer

The previously mentioned device is capable of analyzing an auxiliary signal during a frequency sweep using signal input from an accelerometer or vibrometer. A 'Laser Doppler Vibrometer' (LDV) is a device used to make non-contact vibration measurements of a surface, this allows monitoring of the vibration amplitude which is an accurate representation of the tip displacement. The most common type of LDV is a single point vibrometer and can measure one directional out of place motion. This Vibrometer is generally a two beam laser interferometer that measures the frequency (or phase) difference between an internal reference beam and the test feedback beam. The test beam is directed onto the target, and scattered light from the target is collected and interfered with the reference beam on a photodetector, typically a photodiode [26,27]. This generates an auxiliary signal which is directly connected to the Ultrasonic driver and analyzer device. The device outputs a signal in the form of a transfer function which can be converted into tool tip displacement via the following formula:

$$Transfer\ Function = \frac{Tip\ Displacement}{Input\ Voltage}$$

A sample of the output is shown in the figure below (Figure 16); note that this image was taken directly from the PiezoDrive website [25] and isn't representative of any portion of this project. Further discussion on the use of this is available in a later section of this report (5.0 Physical Testing Results: Mechanical Response)
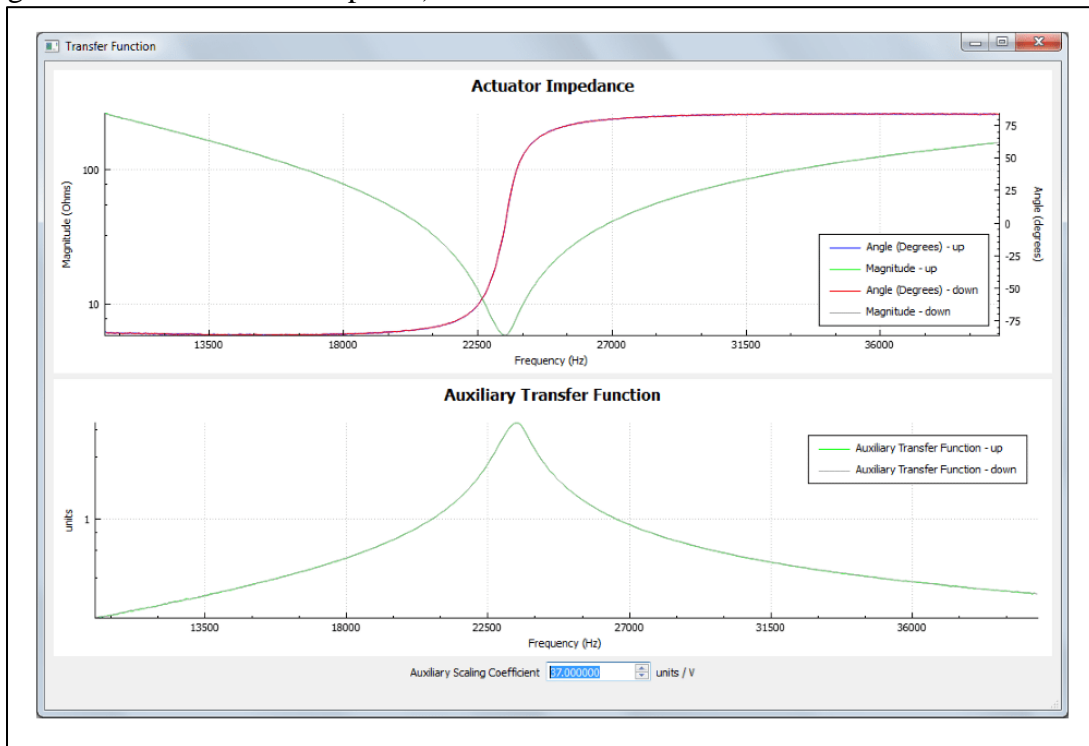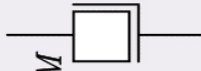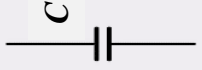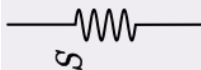

Figure 16: Sample output of frequency sweep with auxiliary signal displacement [23]

4.0 Resonance Frequency Matching

Electrical Response

Matching the frequency of the transducer is a repetitive solution task since requires multiple iterations. The iteration experiments conducted are presented below as separate case studies. The goal was to achieve true resonance between the transducer (vibration source) and the designed horns. As previously stated, this condition occurs when the measured phase angle is zero degrees. Since this is the ideal situation where only the minimal mechanical resistance or damping are present in the system, all other electrical impedances coming from the capacitance and inductance of the system are minimized. The impedance-mobility analogy allows explanation of the occurring mechanical motion system using an analogous electrical system. Where the system is represented by 3 components as shown in the table below (Table 3 [24]).

Table 3: Impedance-mobility analogy symbols with logical meanings

Type	Electrical Symbol	Electrical Meaning	Mechanical Analogy	Mechanical Meaning
Resistance	R	Disspates energy as heat (Ohm's Law)	R_m	Shock absorbing or damping through friction
Inductance	L	Resists change in current, stores energy in magnetic field	M	Added mass or rigid weight (Newton's 2nd Law)
Capacitance	C	Resists change in voltage, stores in electric field	S	Added stiffness or spring (Hooke's law)

It is an undesirable effect to store mechanical energy within the system, in true resonance maximum energy is transmitted through the system. The only effect remaining is by physical system resistance and not impedance from capacitance or inductance. In this report 3 iterations of horns were studied in attempt to produce harmonic electrical resonance and amplify the applied transducer oscillations.

4.1 Case 1: Single Body Steel Conical horn

The first case considered was a steel horn with a conical shape created in a single body format. Intent here was to create a complete horn with high strength and hardness such that it was capable of handling significant impact when processing the aluminum surfaces [25]. This prototype was designed as a cone shape design with basic parameters calculated analytically through MatLab. This resultant analytical calculation model is shown in the figure below (Figure 17), note this horn is designed for 4140 steel with an input end of 70 mm and output of 1 mm.
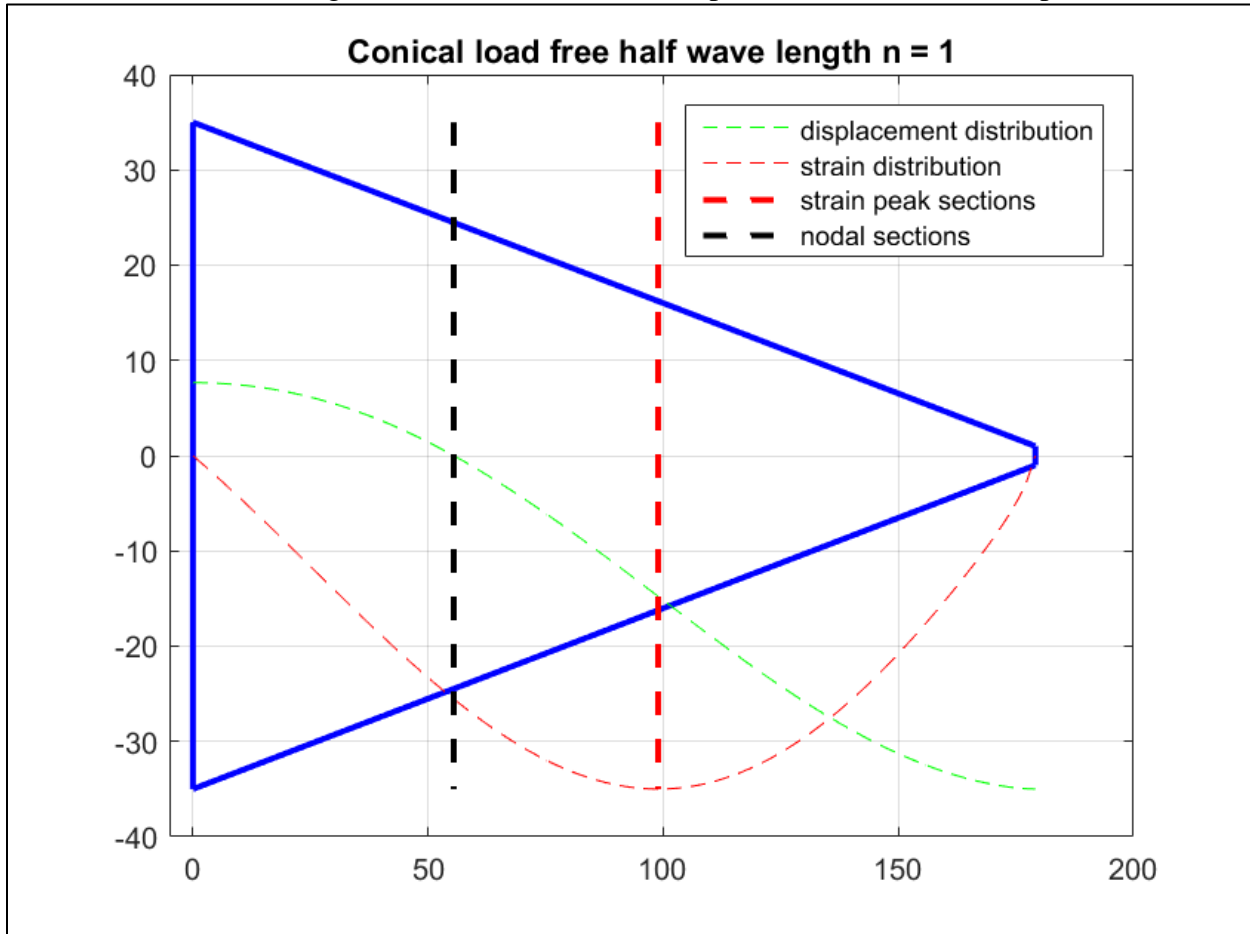
Figure 17: MatLab plot result for steel conical horn, Overall length 179 mm, nodal flange location 55 mm, strain peak location 99 mm

This was converted directly into a 3D model by revolving the shape and adding the mechanical features such as fastening threads, nodal flange, or grip surfaces required for physical assembly. The previously mentioned boundary conditions and mesh settings (see sub-section 2.3 Iterative Numerical Simulation) were used to produce the resultant Eigen-frequency and displacement simulation (Figure 18). The drawings were sent out to the machining center for manufacturing as previously discussed, the final result could now be tested for electrical response via the frequency sweep technique.
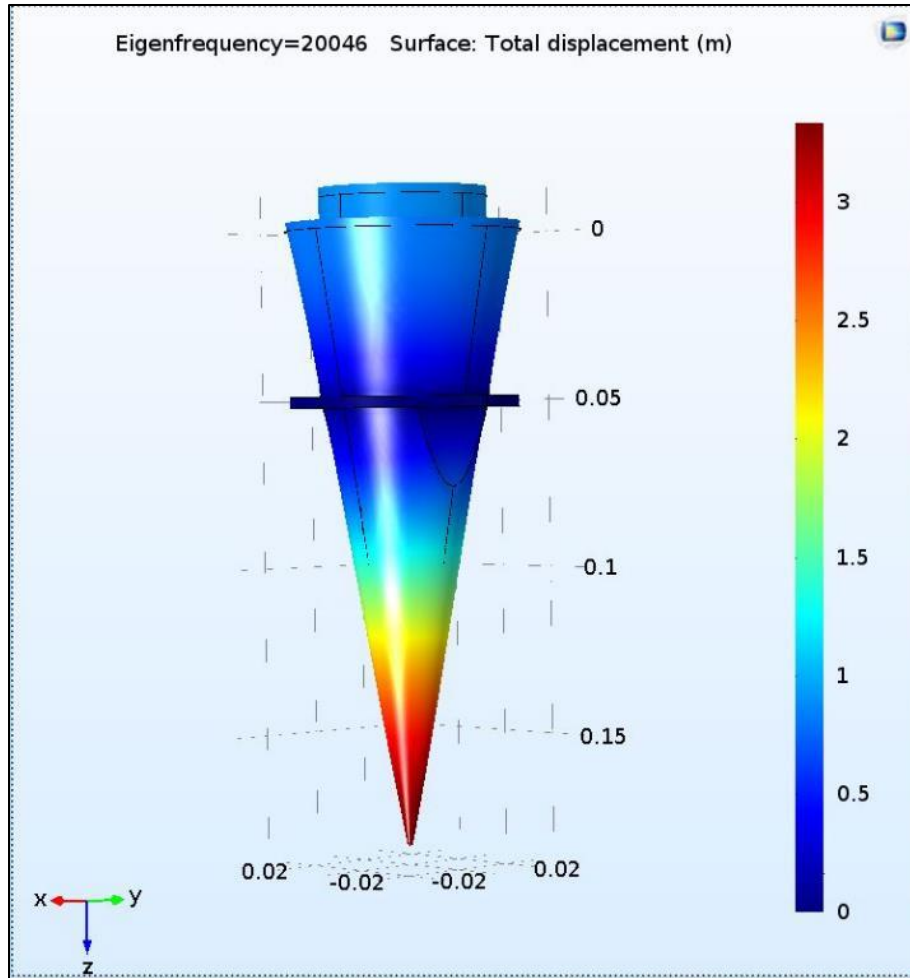
Figure 18: COMSOL plot result for steel conical horn, Overall Length 170.3 mm, Nodal flange location 52 mm, added 10 mm connection to transducer segment

The frequency sweep was conducted between 19 kHz and 22 kHz to allow for a range around the target resonance frequency with fixed 30 V peak to peak applied input voltage. The shape of the plot shows to be correct compared to research however once analyzed further, the phase angle does not reach zero degrees, and the magnitude of impedance is still fairly high. The maximum phase angle reached was approximately -50 degrees which is still in the conductance range. The minimum magnitude of impedance was approximately 250 Ohms, while ideally the system should be expected to produce less than 100 Ohms during true resonance. Therefore, resonance was not achieved using this horn and the reasoning was not completely understood and require to be studied further.

After receipt of the manufactured steel horn device, the research group noted that the device being much heavier than anticipated, weighing approximately 4kg. The mass of the transducer was much smaller (weighing approximately 1kg) since a portion of it used aluminum rather than steel for the whole body. The reasoning behind the use of aluminum segment was to allow for the propagation of oscillations to be in the direction of the less dense, lighter metal section. Therefore, the higher density of steel material led to an overly large mass causing the system to remain in capacitance mode only. Essentially the oscillations were being stopped and bounced back into the aluminum segment of the transducer rather than continuing to the tip of the horn. The record actuator power output from the PiezoDrive software was much smaller (1:10 Ratio) compared to

23

the amplifier power output which explains that the system was storing energy rather than dissipating it as mechanical displacement. The figure below (Figure 19) shows the output of the frequency sweep conducted.
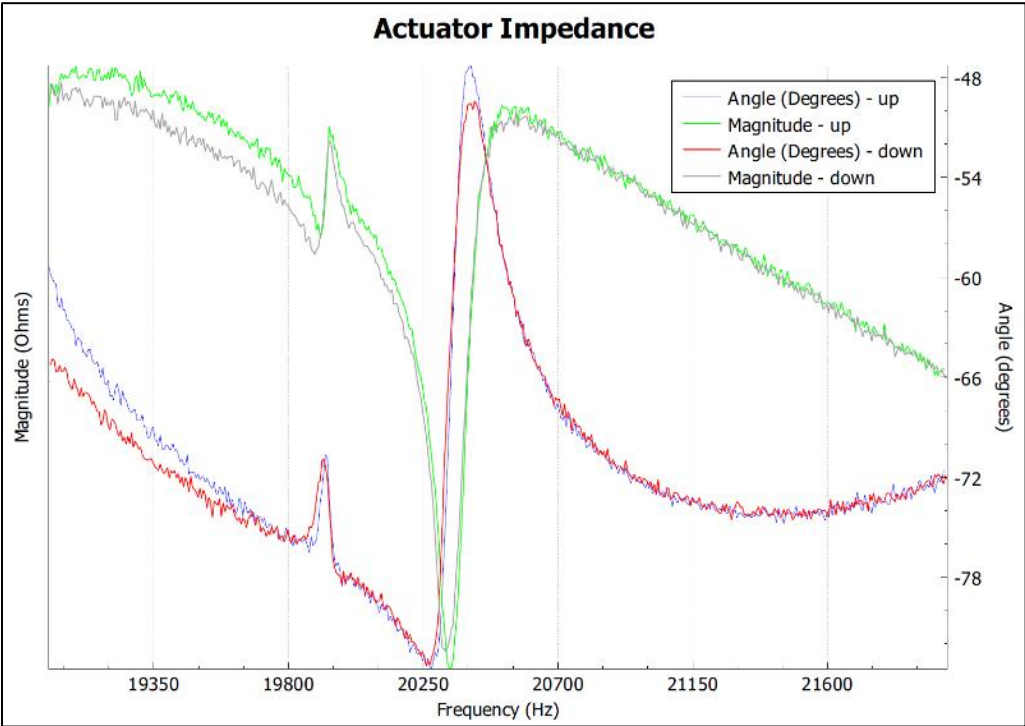

Figure 19: Steel Horn frequency sweep failing to reach resonance

4.2 Case 2: Two Part Aluminum Conical horn with Steel tip

      Based on what was learned from the first steel horn, this iteration was designed to be made from a less dense material (Aluminum 6061). However the tip hardness condition is still required and thus a two part design was implemented. The main body was a conical aluminum portion designed similar to the previous model, with a steel segment attached to harden the tip for processing purposes. The MatLab code does not include two material combination functions, thus this design was partially calculated using the code and remainder modeled numerically calculated. Note that the steel segment was designed to be "bullet" shaped for simplicity of manufacturing; it was also threaded to the main aluminum body (resultant model in Figure 20).
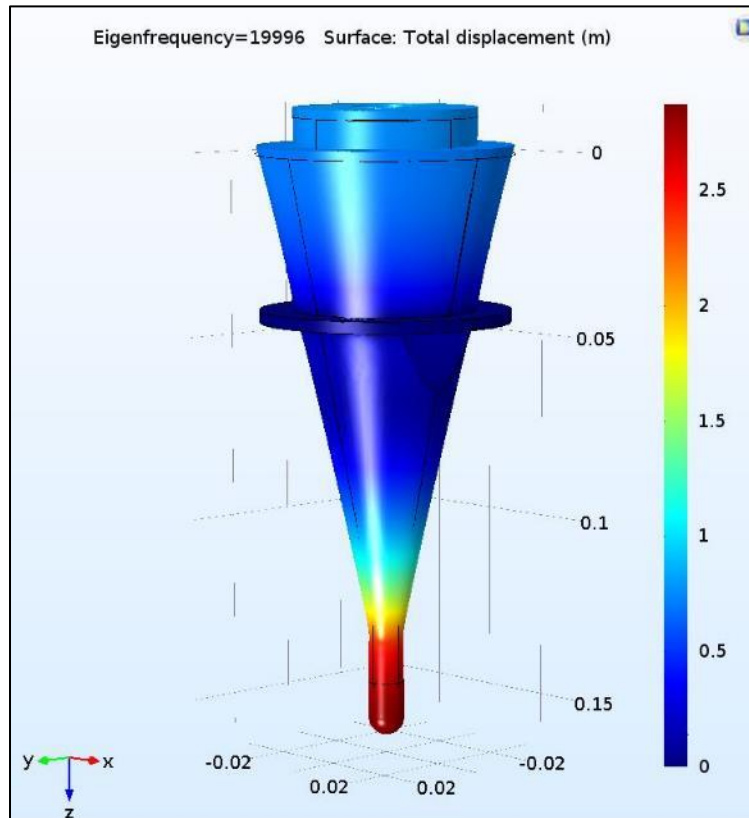
Figure 20: Conical aluminum horn design with steel bullet tip COMSOL numerical result

      The main assumption made during this design is that the steel portion directly affected the resonance of the whole body and caused a reduction in frequency based on the formula:

$$f = \sqrt{\frac{k}{m}}$$

(4.1)

where
k = Wave number
f = Frequency
m = Mass

      This assumption showed to be correct when numerically calculating the Eigen-frequency and the aluminum horn was designed based on those results. Note however, that without the steel

25

bullet tip the resultant horn would be operating at approximately 24.4 kHz which is much higher than the original target of 20 kHz (model without tip Figure 21).

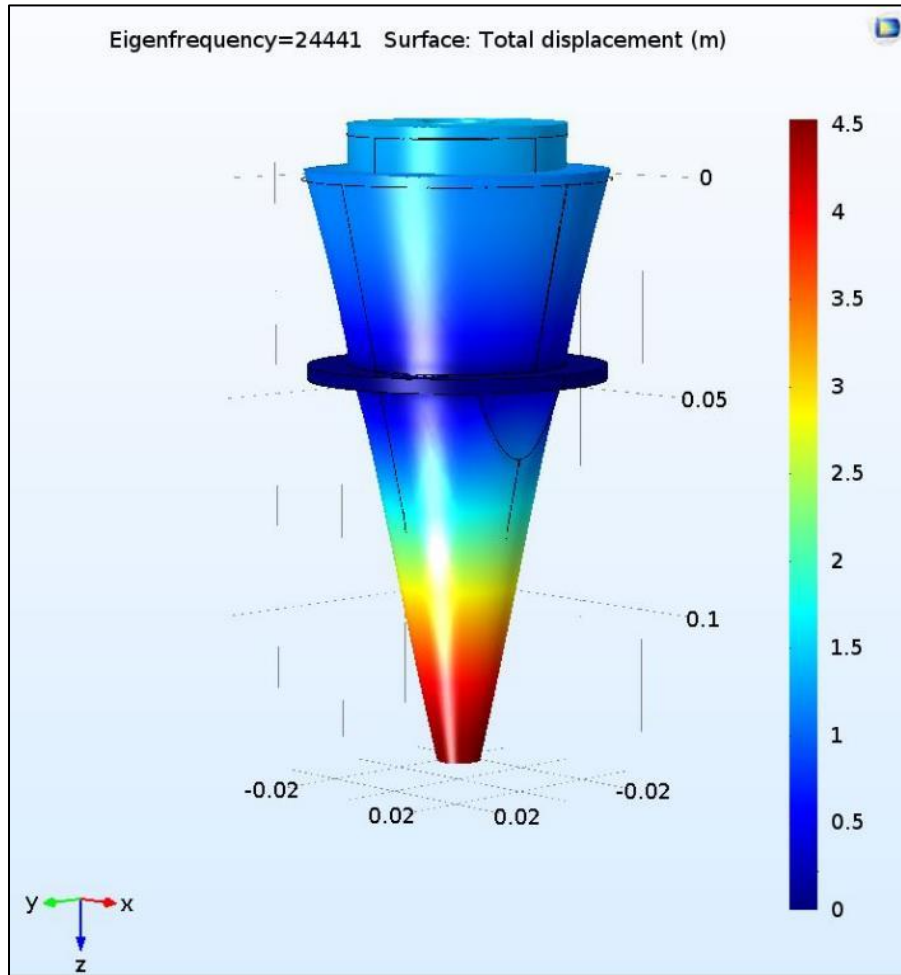*Figure 21: Conical Aluminum horn design without tip attached, COMSOL numerical result*

After manufacturing the horn device, it was tested for electrical response similarly to the case from the previous section (section 4.1). In this iteration however, the result showed that there were two resonance peaks. One of the peaks was similar to the transducer sweep (shown at 20 kHz), and the other seems to be the resonance of this aluminum horn at approximately 23 kHz. The same frequency sweep test was conducted without the steel tip attached and produced an almost identical result. This split in the resonance peak shows that the larger main body portion of the horn is the only contributor to impedance and the attached steel segment has minimal or no direct effect on the system. This may be due to the fact that there is a discontinuity in material between the two parts, which acts as a separate boundary condition. This separation condition was not modelled in the numerical calculation; however, the COMSOL numerical calculation included only a transition of material with the union assembly assumption. The figure below shows the impedance frequency sweeps for both of the tests conducted (Figure 22).
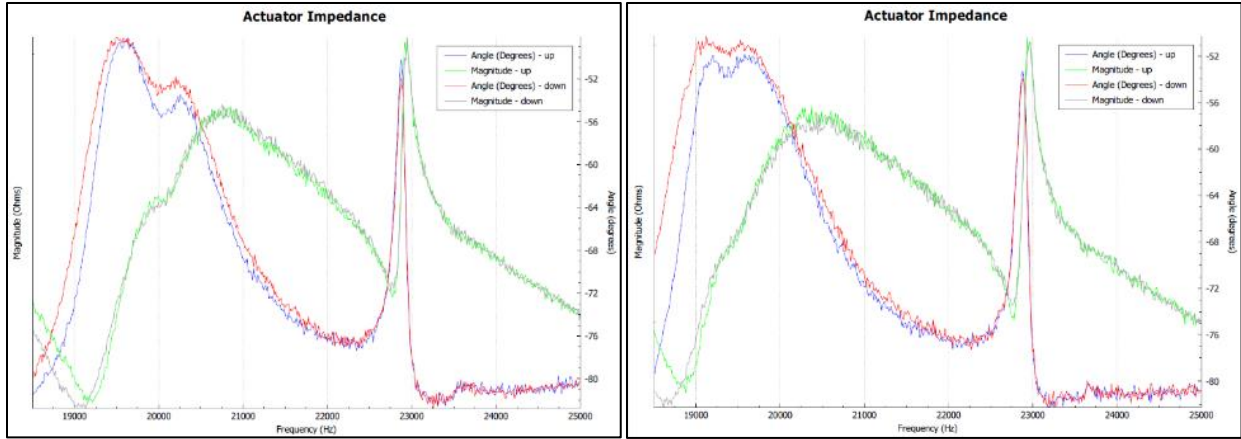
Figure 22: Aluminum horn frequency sweep, with Steel Tip (Left), without steel tip (Right)

It should be noted that the maximum phase angle achieved was in the negative/conductive region (~50 degrees) and the minimum magnitude of impedance was also high (~250 Ohms). Therefore, this iteration of design was not able to achieve resonance despite the original numerical calculation showing that the Eigen-frequency matched the target transducer operation frequency.

4.3 Case 3: Single Body Aluminum Multi-stepped horn

The third iteration was approached in a different manner than the previous two, as there was a complete redesign and change in shape methodology. The research group chose to incorporate a stepped shape design rather than the original cones to simplify manufacturing, thus keeping the work within the scope of the project. The design has a 4 segmented multi-stepped shape, with a decreasing diameter from 50 mm input to the 10 mm at the output end. Since this design was also manufactured from aluminum, the tip end of the device included a threaded hole used to attach various hardened tips such as a carbide dowel and the previously mentioned steel bullet. A more detailed explanation of the development steps of this final design was previously discussed in the section 2.3 (Iteration Numerical Simulation) of this report.

This horn was designed such that the target Eigen-frequency was approximately 20 kHz without any tips attached based on the learnings from the previous iteration (see section 3.1 for figures). It was also tested for electrical response using the same frequency sweep technique between 19 kHz and 22 kHz, the resultant plot is shown in the figure below (Figure 23).
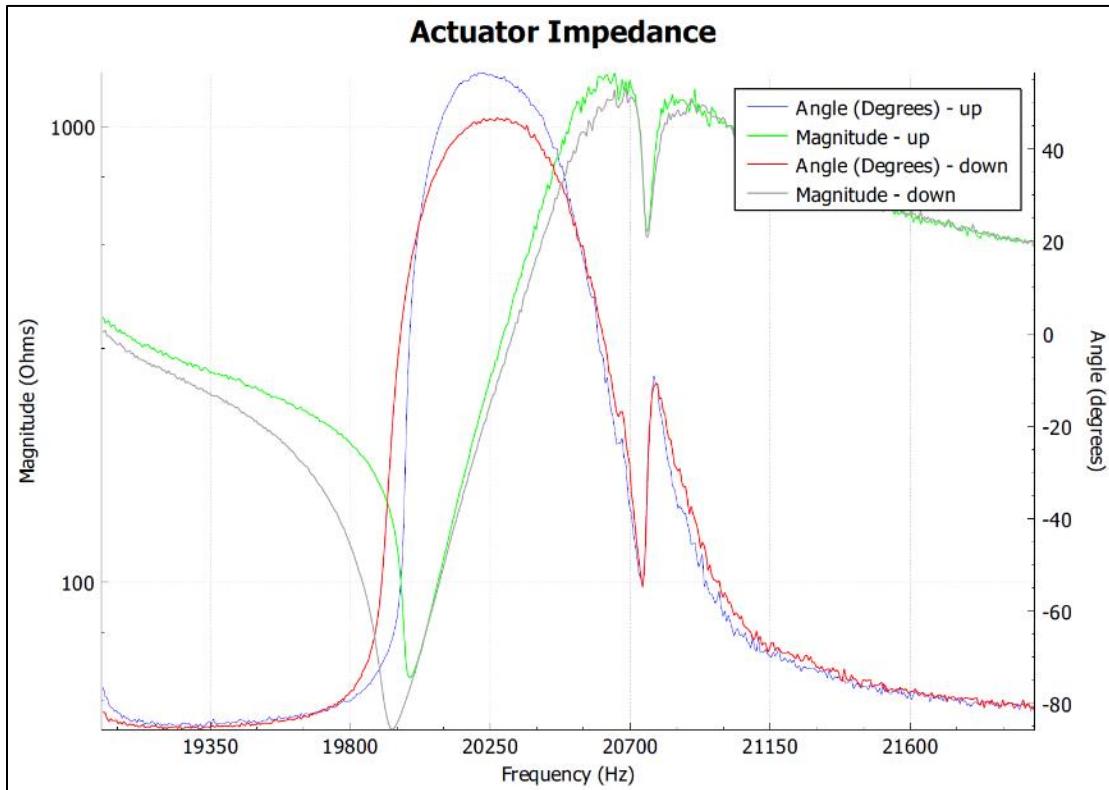

Figure 23: Third Iteration, multi-stepped aluminum horn frequency sweep

The phase angle passes through zero degrees at approximately 20 kHz and the magnitude of impedance is greatly minimized (45 Ohms) at that same point. One aspect of the resultant plot which is not completely understood is the lack of linearity in the sweeps. This is shown as the difference between the up direction test and the down direction test, which seems to be a slight separation between the red and blue curves near the resonance point. This may be due to the poor surface machining quality of the horn or the small gap seen at the attachment surface to the transducer or the theory of physical non-linearity of piezoelectric devices, however the exact reasoning behind this phenomenon was not studied in detail (see Figure 24 of these conditions

28

below). Since true resonance was achieved with this iteration and it was used begin to testing different conditions and experimental setup methods which would occur during surface processing.
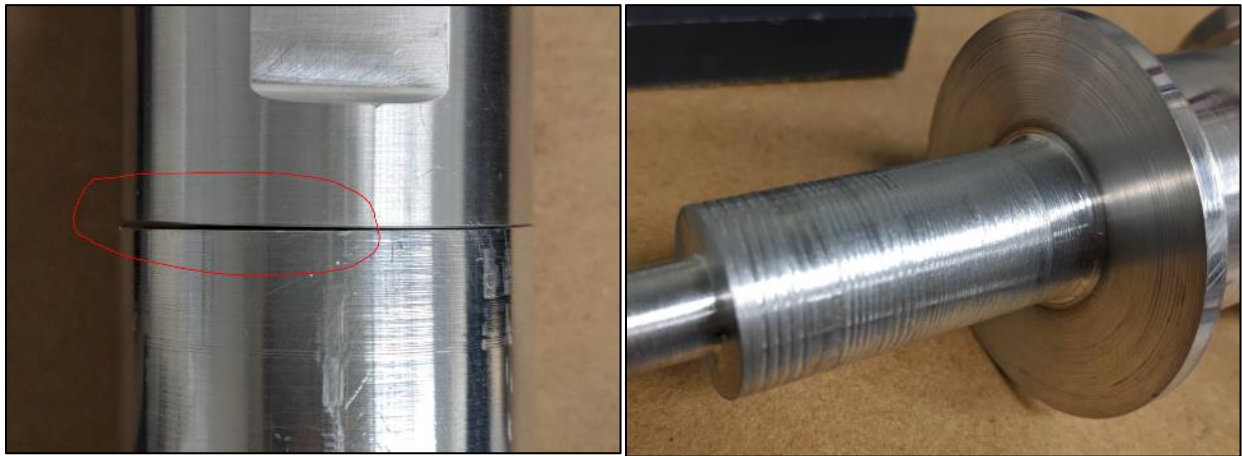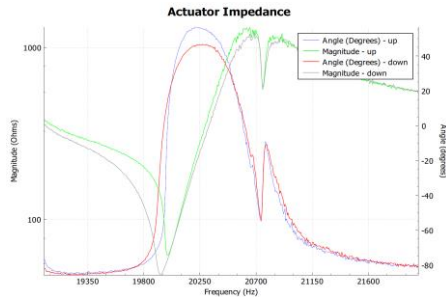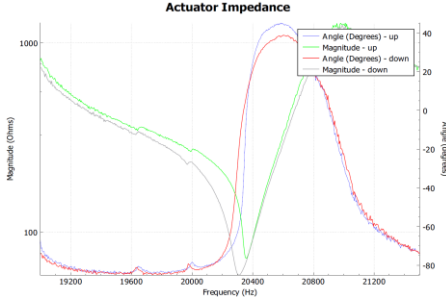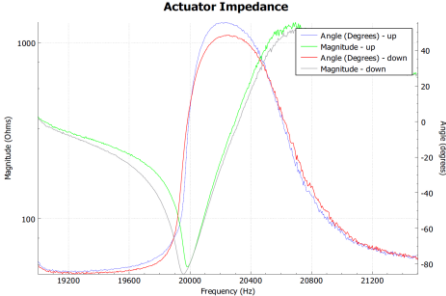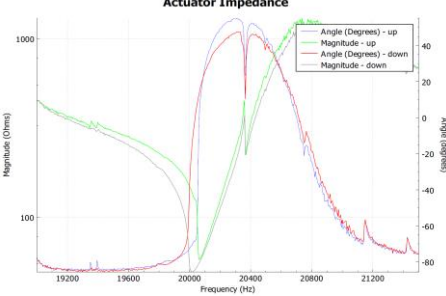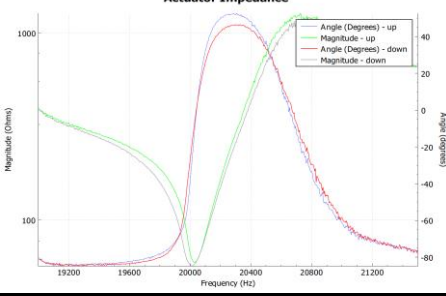

Figure 24: Images showing machining defects which contribute to non-linearity

Effects of Experimental Setup Conditions

First considering the effect of the attached hardened tip such as a 'steel bullet' previously mentioned (Section 4.2). This setup still retained the same overall shape however caused a slight increase in frequency (400 Hz shift right) in the resonance point; this is likely due to the increased length of the system as a whole. Secondly, consider the effects of bringing down the tip of the horn to touch down onto various different surface materials. The three tests conducted were touching onto a wooden block (1 inch thickness), a thick aluminum plate (1/2 inch or 12.7 mm thickness), and a thin aluminum plate (1/8 inch or 3 mm thickness). The results of these studies along with images of the frequency sweeps are summarized in the following table below (Table 4). Note some items still need to be studied further with mechanical response using the laser vibrometer previously discussed in section 5.0 (Physical Testing Results).

Table 4: Effects of Test Setup Condition on Electrical Response in Frequency Sweeps

Test Case Condition	Frequency Sweep Image	Resonance Point (Zero Phase Angle)	Result Notes
Basic Setup (Free/ Fixed)		19990 Hz	Original test conditions, resonance achieved, poor linearity between up and down curves
Steel Tip Attached		20360 Hz	Slight shift in resonance (approx. 400hz), due to increased length of device
Touch onto Wooden Block		19995 Hz	Minimal to no effect compared to original, curve seems to be smoothened overall possible damped system
Touch onto Thick Aluminum Plate		20060 Hz	Minor effect on resonance point (70hz), significant drop seen at (20300 Hz) possible resonance frequency mode of plate
Touch onto Thin Aluminum Plate		20040 Hz	Minor effect on resonance point (70hz), No drops seen and smoothened overall shape

5.0 Physical Testing Results

Mechanical Response

As previously discussed (section 3.2), a laser vibrometer was used to measure the mechanical response of the horn and transducer during operation. The auxiliary signal output is sent to the piezo-drive analyzer and output is seen as a transfer function, this transfer function can be converted into a physical displacement based on the signal to voltage sensitivity and the applied input voltage. The sensitivity was arbitrarily set to 1 micrometer per volt, such that the conversion mathematics would be simplified in later analysis of the collected data. Due to the functionality setup of the LDV (attached to a tripod fixture), it was required to place the ultrasonic device in a flipped direction such that the tip of the horn would be facing the LDV (upwards). The gravitational load of the transducer had no effect on these measurements since the device was fixed to the CNC by the nodal flange on the horn itself. This assumption can also be proven by removing or altering the boundary condition of transducer weight which was originally applied in the finite element models [26,27].

To attempt to understand the results of the previous electrical response this laser mechanical response experiment was conducted with 3 different setup modes: no tip attached, aluminum tip (carbide dowel holder) attached, and steel tip ("steel bullet segment) attached. Note that the carbide dowel was removed from the end of the devices since its surface area was too small to reflect the laser and provide a sufficient analysis signal. A sample of the resultant auxiliary transfer function plot compared to the actuator impedance during a frequency sweep is shown in the figure below (Figure 25).
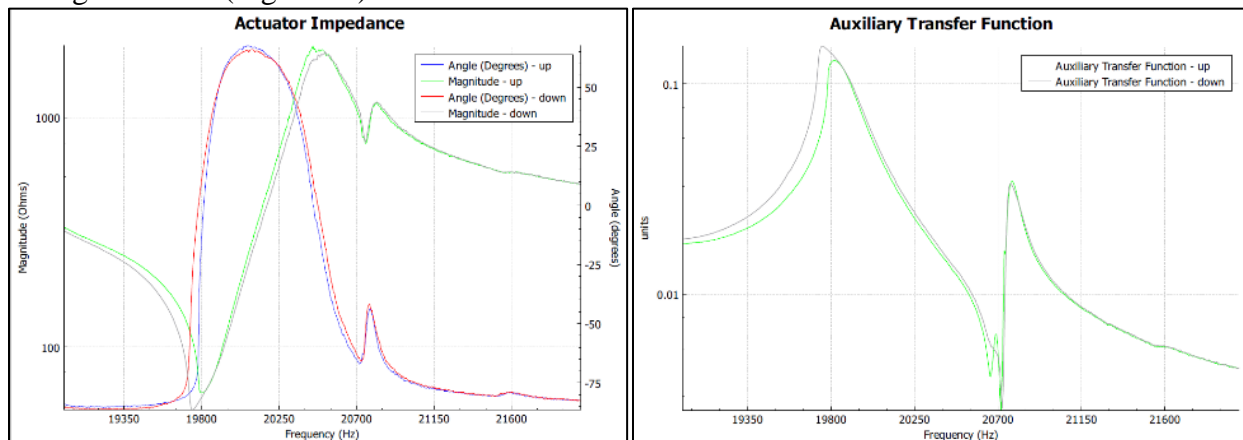

Figure 25: Auxiliary Transfer Function (Right) compared to Actuator Impedance (Left) during Frequency Sweep

The peak of the auxiliary transfer function is located at roughly the same location as the zero phase angle resonance point, this is the expected result and means that the largest displacements will occur during system resonance. There are two items which were less expected to occur but should be noted:

- Non-linearity previously discussed (difference between up and down curves)
- System instability which occurred when attempting to conduct tests at higher voltages

Based on research of piezoelectric devices, it is possible that these two items are correlated and appear to have a more significant impact when operating at higher applied voltages. Some papers discus that there can be a mathematical error due to neglecting the physical non linearity of a piezoelectric device in dynamic formulations [28,29]. Essentially, the effect of physical nonlinearity on the dynamic response of piezoelectric devices which are polarized (in the axial direction) and subjected to an applied input voltage. It was shown that physically nonlinear effects

become more pronounced at higher input power levels. While mathematically, the nonlinearity results in additional terms in the system of equations, such that the equations to mixed forced-parametric dynamic formulation (Mathieu-Hill equations) [28,29]. The error due to neglecting the physical nonlinearity may be significant in some cases since this error increases when close to the resonant frequency. Also noted was that the inaccuracy of the linear analysis increases at higher applied input power [28,29,30].

Fortunately, the effect is not very significant at approximately 30 Hz (~1% error) during low voltage applications such as the experiments conducted here. The maximum applied voltage was limited to 120V peak to peak as a precaution for testing purposes. However with the steel bullet tip attached, the system instability seemed to appear at lower voltages as well and decreased the signal to noise ratio of the auxiliary signal which lead to an undistinguishable data set.

5.1 Data Trends of Results

Tests for no tip attached and aluminum holder attached were conducted at variously applied input voltages ranging from 5V to 120V (peak to peak). The results show very similar trends with a minor damping factor due to the added mass and length of the attachment. This is shown first by plotting the transfer function maximum point compared to input voltage shown in the figure below (Figure 26). This result shows a trend of slight decrease in this maximum transfer function point with increasing applied voltage.

Note: To reduce outlier noise on the test results, all points collected for one voltage setup (multiple tests and up/down curves) were averaged within the dataset. Each of the parameters plotted in this section are calculated based on the refined average results.
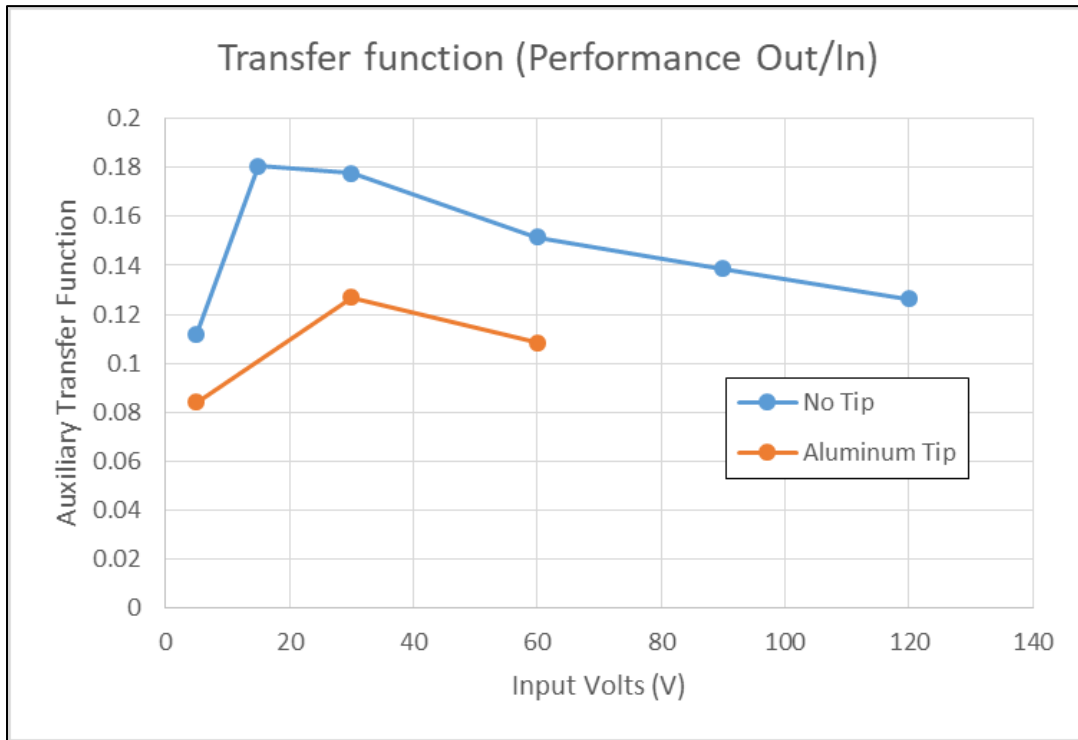

Figure 26: Maximum Transfer Function Compared to Applied Input Voltage

However, the auxiliary transfer function is a non-dimensional entity, which is represented as output over input as such:

$$T_F = \frac{Output}{Input}$$

This can be converted to a physical tip displacement using the previously mentioned system sensitivity (1µm/V). Therefore rearranging this to calculate tip displacement can found by multiplying the transfer function by the applied input voltage as:

$$Tip\ Displacement(\mu m) = Transfer\ Function\left(\frac{\mu m}{V}\right) \times Input\ Voltage(V)$$

Shown in the figure below (Figure 27) is the calculated tip displacements corresponding to the above mentioned transfer function calculations.
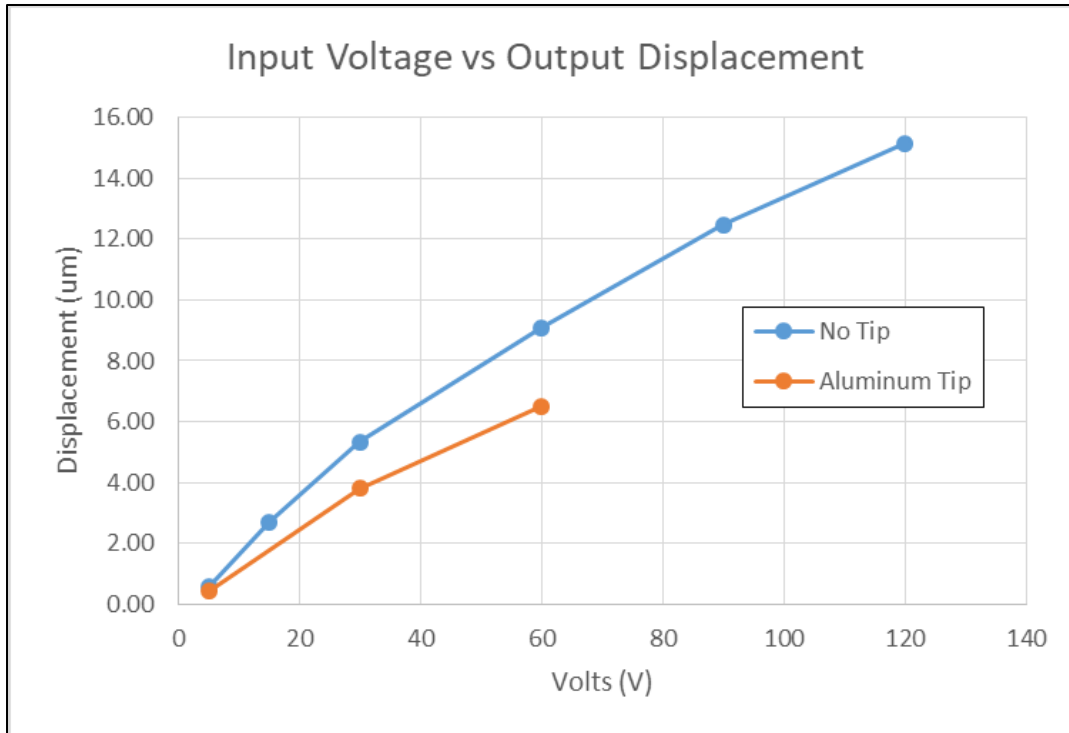
33

Figure 27: Calculated Tip Displacement Compared to Applied Input Voltage

Another trend found from this plot is there is a non-linear increase in displacement, likely meaning that the decay in transfer function noted previously is due to performance limitations of the transducer itself when higher applied voltages. This also leads to the conclusion that there may be an asymptote point where the maximum displacement no longer increases significantly with applied input voltage.

The final comparison studied was point of occurrence for the maximum transfer function (or displacement) and how it is affected by changing frequency, phase angle, or input voltage. In these figures below (Figure 28, Figure 29) the point of maximum displacement is compared to both phase angle and frequency at the various applied voltages. It was found that the points (on average) occur near the zero phase angle resonance point however there is a slight tendency to shift towards the negative phase angle side (capacitance mode) [24]. This allows to conclude that processing operations should be conducted by tracking of roughly -10 degree phase angle rather than the exact resonance point of zero degrees. From the frequency comparison it can be noted that the system resonance remains at a close values across various voltages with a minor decrease of 400 Hz over the whole range (5 V to 120 V). There is also a significant difference between system frequencies at the maximum point when comparing the aluminum tip data set to the base system without any attachments. This is due to the length of the device changing and causing a resonance shift in the impedance sweep curves as previously noted.
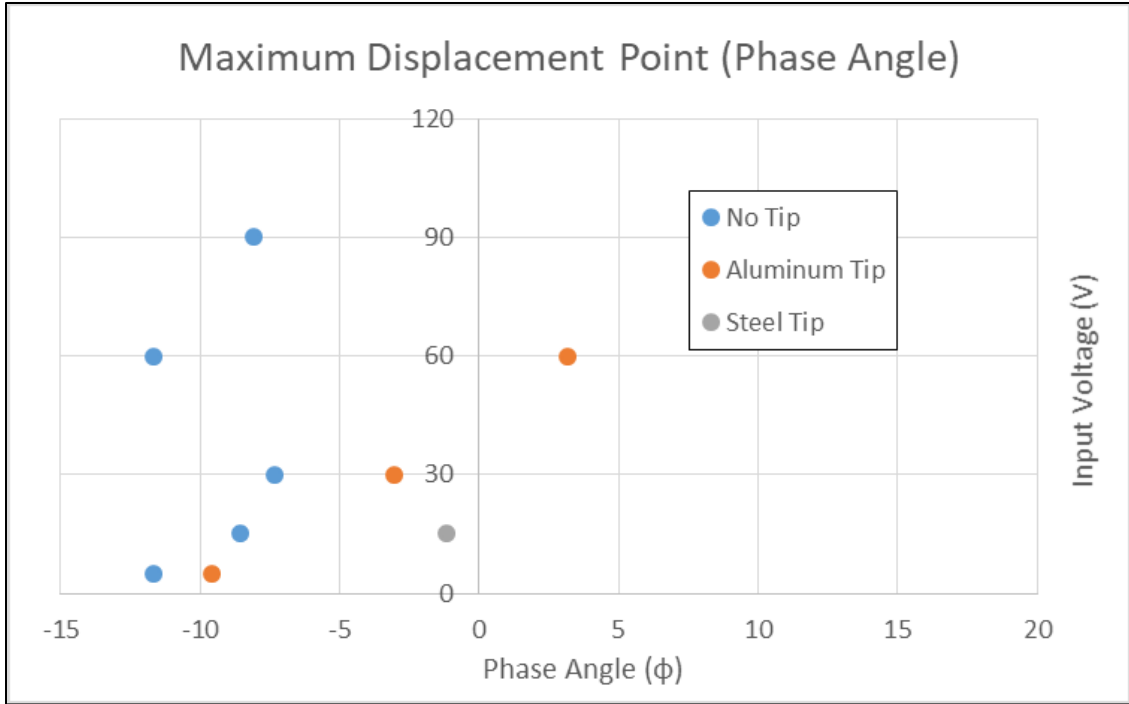
Figure 28: Maximum Displacement Point Comparison by Phase Angle vs. Applied Input Voltage
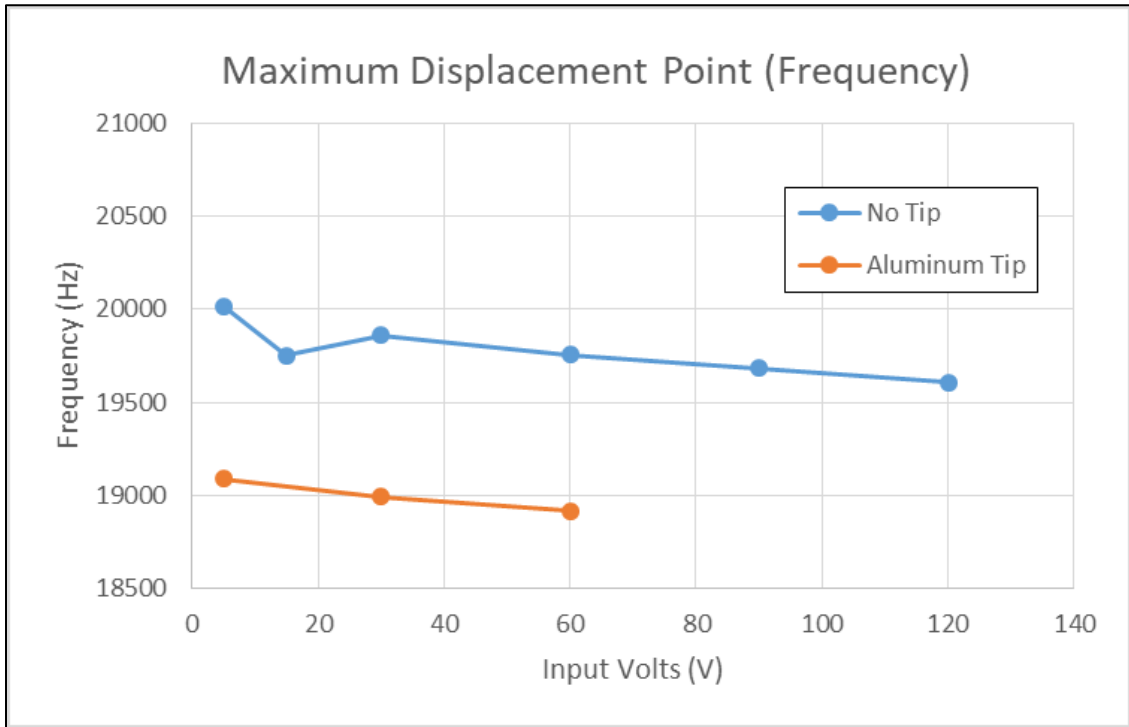

Figure 29: Maximum Displacement Point Comparison by Frequency vs. Applied Input Voltage

6.0 Surface Processing Results

Processing Setup Parameters

  The objective of this study was to develop the devices capable of creating compressive residual stress fields on the surface of a metal sample. This section describes the experiments conducted in attempt to pattern an aluminum surface and the findings associated with these tests.

  Beginning with choosing an appropriate material for processing, the optimal material seemed to be a thin plate of aluminum since it showed the least significant effect on impedance response and was readily available as scrap metal. Using a thicker and larger sample of aluminum may have been more helpful in keeping the sample stable and withstand the downward forces of the processing without much other clamping required, however this would require more wasted material in the preliminary tests required to optimize the experiments.

  Firstly, preliminary experiments were conducted including setup of tool path pattern to determine optimal size parameters, choosing between flat-bottom versus rounded ball-bottom tip of the carbide insert, and use of free z-axis assembly fixture. These items were all tested through different setup combinations to produce the most useful resulting setup which was later used to produce the measured samples. When using the smaller tipped ball end of the carbide insert the surface, this created a pattern which a set of lines rather than covering whole test area surface (approximately 1cm^2). However, to accommodate for this it was possible to bring the lines closer together by adjusting the tool path of the device, this meant that processing time increased to process the same small area. Therefore, the decision to use the larger flat bottom of the carbide insert (full circular diameter) was deemed the most practical and only a half overlap of the tool diameter was necessary to create a complete surface pattern.

  The second major setup issue came into consideration when it was noticed that the static friction on the free z-axis assembly was larger than force generated by moving across the metal surface, which caused the horn assembly to bend near the tip rather than slide when attempting to move around with the complete weight of the setup placed down onto the fixed samples. To reduce the bending effect in attempt to keep the horn tip flat and perpendicular to the sample surface, the free z-axis assembly was removed and the flange clamp portion was fixed, directed and constrained to the exact movement of the CNC tool arm. Due to this setup the z-axis motion is now limited to the exact movement precision of the CNC Z axis, which is only able to move with 10 µm steps of minimum accuracy. Previously it was noted that the oscillations of the horn tip would be smaller than 10 µm when applying lower input voltage (<100V peak to peak). This made setting up the optimal Z height of the tool not possible since all tests needed to be conducted under 100V for safety and stability reasons. However, this also meant that many samples had to be discarded or repeated due to the tool tip being too far away or pressing too deep into the sample surface.

Measurement of Processed Surfaces

  After resolving the above mentioned setup parameters it was possible to produce a surface sample which was usable for measurement. This sample was created by using a continuous processing technique with 4 smaller interval sections of 1 cm^2 area side by side under different input voltage conditions (see Figure 30 below). Using this technique allowed the Z axis point to be held constant while continuous movement was possible without the requirement to stop after each section program to adjust the applied input voltage.
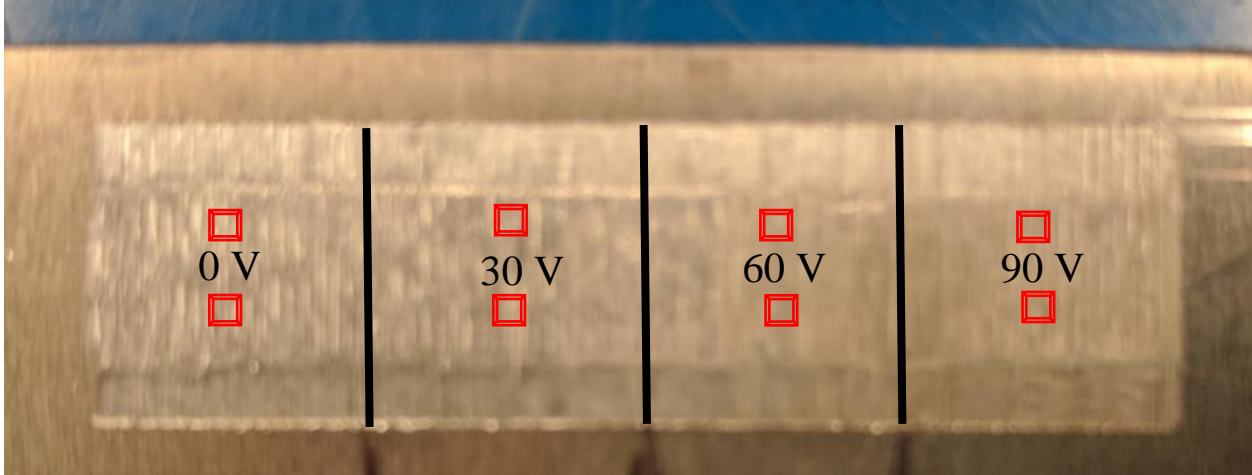
Figure 30: Image of continuous processing technique with various input voltage tests labeled for 4 different 1cm2 intervals and measurement points

Multiple other unsuccessful samples are not included in this report since detailed data was not collected on them, they were used as visual reference to help create this final processed sample. This sample was analyzed using a Veeco optical surface profiling system which uses red light (selects 621nm wavelength of white light) diffraction technique to measure the depth of multiple points [13]. Veeco's product information for the device mentions that, "a white-light beam is filtered and passed through an interferometer objective to the test surface. The interferometer beam splitter reflects half of the incident beam to the reference surface within the interferometer" [31]. During measurement, a piezoelectric transducer (PZT) linearly moves the reference surface a small known distance to cause the phase shift in the beams which is measured. The system records the intensity of the resulting interference pattern at many points, and then converts these to applicable data by integrating the function [31].

Using this device it is possible to produce 2 and 3 dimensional measurement images with very high accuracy (close to 10nm). The sample above was tested for 2 different measurement areas (approximately 1 mm^2 in size) in each applied voltage section as indicated by the red squares in the figure above (Figure 30). The output result images of all the measurement areas are attached in appendix D, however there are some specific items which can be summarized and noted about the differences.

Analysis and Comparison of Measured Areas

The software automatically calculates roughness parameters based on the measured area, these are described from the operation manual as follows [32]:

Ra: The average roughness calculated over the entire measured array.

$$R_a = \frac{1}{MN} \sum_{j=1}^{M} \sum_{k=1}^{N} |Z_{jk}|$$

(6.1)

Rq: The root-mean-squared roughness calculated over the entire measure array.

$$R_q = \sqrt{\frac{1}{MN} \sum_{j=1}^{M} \sum_{k=1}^{N} Z_{jk}^2}$$

(6.2)

Rz: The Ten-Point Height. The average of the ten greatest peak-to-valley separations in the evaluation area

$$R_z = \frac{1}{10}[(H_1 + H_2 + \cdots + H_{10}) - (L_1 + L_2 + \cdots + L_{10})] \tag{6.3}$$

Rt: The difference between the maximum and minimum points in the entire measure array.

$$Rt = Zmax - Zmin \tag{6.4}$$

These roughness parameters could be more useful if the whole measured sample array did not contain any significant defects, however there are multiple instances of areas in the samples tested which detract from the usefulness of these calculated figures. In some of the tested sample areas there seems to be a large valley indicated by dark blue section, which was created by small surface debris being dragged under the tool tip during processing (see Figure 31 below).
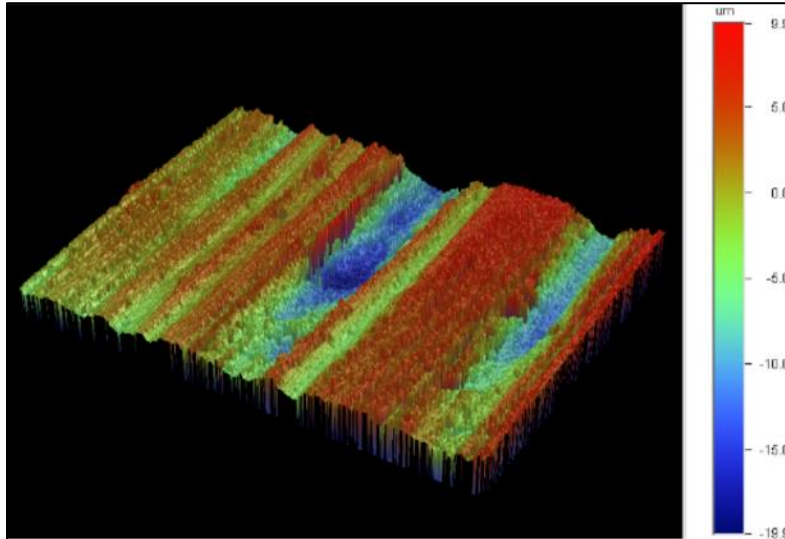

Figure 31: 3D Image of large defect area in surface processing caused by debris

Based on the values of the roughness parameters measured for the samples, specifically Rz (see Table 5 below), it is possible to conclude that there was a trend of increasing roughness when applied voltage is increased. This trend is a correlated to increased tip displacement (0 µm, +3 µm, +6 µm, +9 µm) if the base roughness is considered as 15 µm (Average Rz value of unprocessed). Other parameter (Ra, Rq, Rt) trends are minor and inconclusive across varying applied voltage due to the debris defects which occurred.

Visually, the zero voltage or unprocessed area simply shows constant scratches with minimal oscillation influence. However, the processed areas show more variation across each peak and valley, indicative of the tip vibration influence. This proves that some compressive residual stress was left present in the area with higher applied voltages were used compared to the area where no applied voltage was used. To improve and further study these results a more accurately moving CNC (<1µm precision) which would have allowed the tip to glide across the surface gently when no voltage is applied rather than create the fine scratches which were observed (see Figures 32 and 33 below).

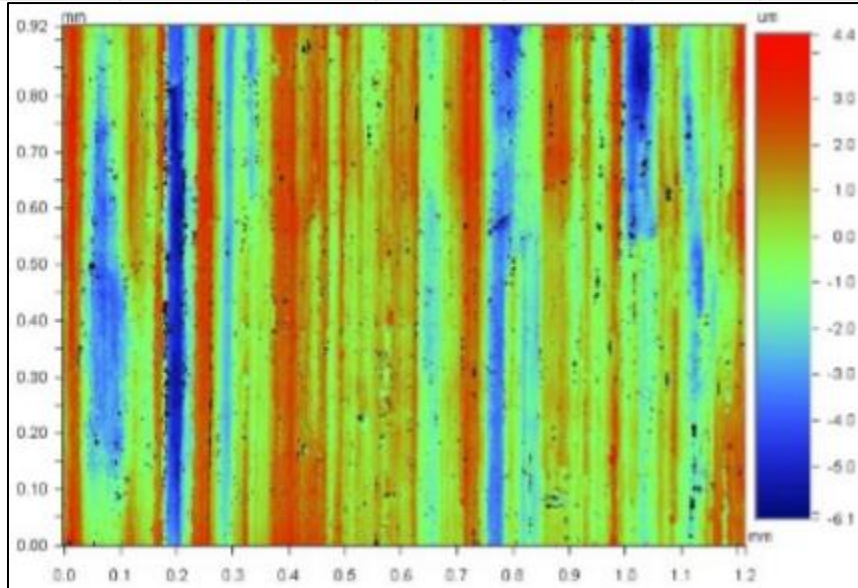| Sample	Ra	Avg Ra	Rq	Avg Rq	Rz	Avg Rz	Rt	Avg Rt
0 V(A)	1.43	2.19	1.79	2.78	10.22	15.15	10.52	15.72
0 V(B)	2.95		3.76		20.07		20.91	
30 V(A)	2.26	2.69	2.70	3.17	16.13	17.71	18.95	20.48
30 V(B)	3.11		3.64		19.28		22.00	
60 V(A)	2.07	2.43	2.81	3.17	16.51	19.32	16.42	19.74
60 V(B)	2.79		3.52		22.12		23.05	
90 V(A)	3.57	3.16	4.76	4.09	28.56	24.37	29.75	25.37
90 V(B)	2.75		3.41		20.18		20.99	

Figure 32: 2D image profile showing scratches seen in zero applied voltage area
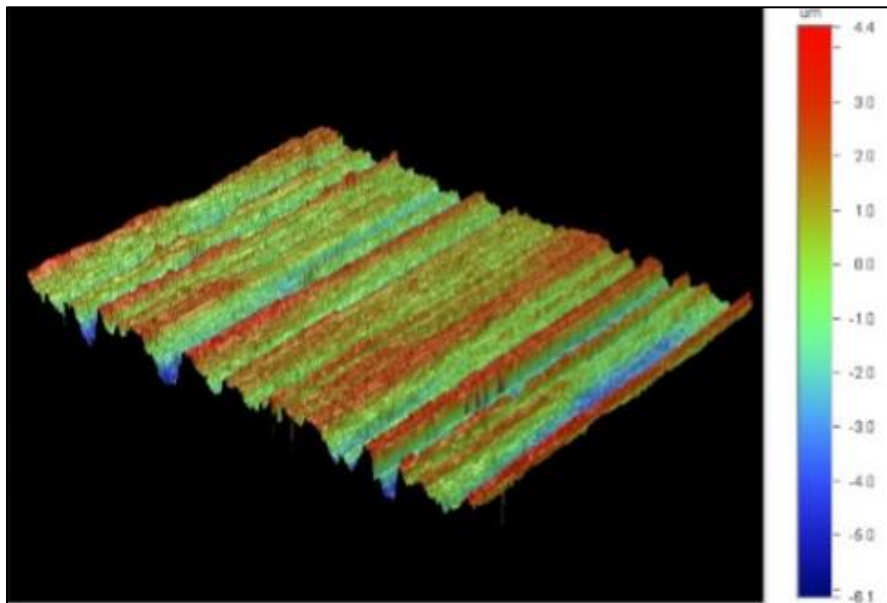

Figure 33: 3D image profile showing scratches seen in zero applied voltage area

7.0 Conclusion

The design of an ultrasonic surface processing device capable of producing compressive residual stress field on aluminum sample is possible. However, it requires detailed development of resonance horns and a significantly high applied input voltage from a power source capable of driving a piezoelectric transducer.

The development of the horn or sonotrode device is important for achieving true resonance such that amplitude of oscillations at the tip end of the device can be maximized. This development process requires analytical and numerical calculations followed by iterative design and manufacturing. Material selection is an important factor that directly influences horn performance, specifically the density and overall mass of the device contribute to its electrical response impedance.

The input power requirements increase directly with the need for larger tip oscillations, thus improving processing times requires high applied input voltages (>60 V peak to peak). Safety issues may arise with significant increased applied input voltage such as instability and excess potential electric energy storage within the device. These issues become limitations of usage if the ultrasonic surface processing device is poorly designed or manufactured. Extensive testing of various resonance conditions should be considered as different tip applications and loads present during processing have a direct effect on the performance of the device. Lastly, the mechanism which controls the movement of the system requires very high precision motion (greater than minimum oscillation displacement of the device) to allow smooth surface processing rather than producing unnecessary damage such as scratches to the sample.

7.1 Recommendations

Cylindrical specimens which can be processed and tested for fatigue life and fracture strength should be considered as the use of semi-destructive testing would prove this techniques industry value. These tests typically use cyclic loading to determine the fatigue life of the specimen, which mimics the long term life of a component in industry. Residual stress testing using surface strain gauge techniques can also be helpful. The shape type of the horn was selected due to practicality and simplicity of this research project, future research and development should consider using multiple shape types in combination to minimize single shape design limitations. Acquiring or designing a Langevin ultrasonic transducer capable of withstanding high applied input voltages (>120V peak to peak) may help in increasing tip displacement oscillations. A corresponding high power source which can provide the system with the requirements is also suggested. From the CNC motion aspect, a study of various feed rates could allow larger distances between scratches which would help prove CRS occurrences. Successful completion of this project will lead to further studies on UST such that it may be used as a full scale mass production process. While learnings from this project can be used to improve mechanical, fatigue, and wear properties, leading to a size reduction and lightweight design of multiple industry products including automotive, manufacturing, and biomedical applications.

8.0 <u>References</u>

[1] M. Torres and D. Harada, "Effect of Shot Peening on Fatigue Behavior of AISI 4340 in Different Loading Conditions", Key Engineering Materials, vol. 713, pp. 30-33, 2016.

[2] Y. Qian and H. Kwon, "Development of Ultrasonic Surface Treatment Device", in CANCAM, London, Ontario, 2015.

[3] H. Al-Budairi, "Design and analysis of ultrasonic horns operating in longitudinal and torsional vibration.", Ph.D, University of Glasgow, 2012.

[4] A. Gujba and M. Medraj, "Laser Peening Process and Its Impact on Materials Properties in Comparison with Shot Peening and Ultrasonic Impact Peening", Materials, vol. 7, no. 12, pp. 7925-7974, 2014.

[5] Y. Choi, K. Park, Y. Hong, K. Kim, S. Lee and H. Choi, "Effect of ultrasonic vibration in grinding; horn design and experiment", International Journal of Precision Engineering and Manufacturing, vol. 14, no. 11, pp. 1873-1879, 2013.

[6] S. Takeda, I. Morioka, K. Miyashita, A. Okumura, Y. Yoshida and K. Matsumoto, "Age variation in the upper limit of hearing", European Journal of Applied Physiology and Occupational Physiology, vol. 65, no. 5, pp. 403-408, 1992.

[7] L. Miller and A. Surlykke, "How Some Insects Detect and Avoid Being Eaten by Bats: Tactics and Countertactics of Prey and Predator", BioScience, vol. 51, no. 7, p. 570, 2001.

[8] J. Tougaard, L. Miller, A., Simmons, J. A. Thomas, Advances in the study of echolocation in bats and dolphins University of Chicago Press, s. 365-372, 2003

[9] A. Peshkovsky, S. Peshkovsky and S. Bystryak, "Scalable high-power ultrasonic technology for the production of translucent nanoemulsions", Chemical Engineering and Processing: Process Intensification, vol. 69, pp. 77-82, 2013.

[10] L. Jeffus, Welding principles and applications. Clifton Park, N.Y.: Delmar Cengage Learning, 2012.

[11] R. Fathallah and H. Sidhom, "Effect of surface properties on high cycle fatigue behaviour of shot peened ductile steel", Materials Science and Technology, vol. 19, no. 8, pp. 1050-1056, 2003.

[12] "Prediction about short fatigue crack growth in compressive residual stress field", International Journal of Fatigue, vol. 15, no. 6, p. 536, 1993.

[13] K. Xu, N. Hu and H. Zhou, "Prediction of notch fatigue limits in a compressive residual stress field", Engineering Fracture Mechanics, vol. 54, no. 2, pp. 171-176, 1996.

[14] K. Dalaei and B. Karlsson, "Influence of shot peening on fatigue durability of normalized steel subjected to variable amplitude loading", International Journal of Fatigue, vol. 38, pp. 75-83, 2012.

[15] M. Malaki and H. Ding, "A review of ultrasonic peening treatment", Materials & Design, vol. 87, pp. 1072-1086, 2015.

[16] H. Miao, D. Demers, S. Larose, C. Perron and M. Lévesque, "Experimental study of shot peening and stress peen forming", Journal of Materials Processing Technology, vol. 210, no. 15, pp. 2089-2102, 2010.

[17] A. Abdullah, M. Malaki and A. Eskandari, "Strength enhancement of the welded structures by ultrasonic peening", Materials & Design, vol. 38, pp. 7-18, 2012.

[18] M. Nad', "Ultrasonic horn design for ultrasonic machining technologies", Applied and Computational Mechanics, vol. 4, pp. 79-88, 2009.

[19] "Steel material properties", Steelconstruction.info, 2017. [Online]. Available: https://www.steelconstruction.info/Steel_material_properties. [Accessed: 14- Mar- 2017].

[20] R. Chaudhuri, Waves and oscillations. New Delhi: New Age International Ltd., 2010.

[21] D. Inman, Engineering Vibrations. Boston: Pearson, 2014.

[22] D. Logan, A first course in the finite element method. Stamford, CT: Cengage Learning, 2012.

[23] "PDUS200 - 200W Precision Ultrasonic Driver & Analyzer", Piezodrive.com, 2017. [Online]. Available: https://www.piezodrive.com/drivers/pdus200-200w-precision-ultrasonic-driver-and-analyzer/. [Accessed: 07- Mar- 2017].

[24] M. Kleiner, Electroacoustics. Boca Raton, Fla.: Taylor & Francis, 2013.

[25] J. Marteau and M. Bigerelle, "Relation between surface hardening and roughness induced by ultrasonic shot peening", Tribology International, vol. 83, pp. 105-113, 2015.

[26] "Single-Point Vibrometers", Polytec.com, 2017. [Online]. Available: http://www.polytec.com/us/products/vibration-sensors/single-point-vibrometers/. [Accessed: 17- Sep- 2017].

[27] M. Chen, J. O'Sullivan and N. Singla, "Laser Doppler Vibrometry Measures of Physiological Function: Evaluation of Biometric Capabilities", IEEE Transactions on Information Forensics and Security, vol. 5, no. 3, pp. 449-460, 2010

[28] V. Birman, "Physically Nonlinear Behavior of Piezoelectric Actuators Subject to High Electric Fields", *United States Army Research Office*, St. Louis, Missouri, 2005.

[29] U. Kushnir and O. Rabinovitch, "Non-linear Piezoelectric and Ferroelectric Actuators — Analysis and Potential Advantages", Journal of Intelligent Material Systems and Structures, vol. 19, no. 9, pp. 1077-1088, 2008.

[30] A. Achuthan, A. Keng and W. Ming, "Shape control of coupled nonlinear piezoelectric beams", *Smart Materials and Structures*, vol. 10, no. 5, pp. 914-924, 2001.fds

[31] "Manual for Optical Profiler Veeco Wyko NT1100", 2017. [Online]. Available: https://cmi.epfl.ch/metrology/Wyko_NT1100.php. [Accessed: 14- Nov- 2017].

[32] Veeco, "Operation Manual: Optical Profiling System Wyko NT-1100", 2006.

Appendix A: Analytical Calculations for Strain Distribution and Maximum Strain [3,21]

$$M_p = \left| \frac{\xi_2}{\xi_1} \right|$$

$$\alpha L = \frac{N-1}{N}$$

$$M_p = \left| N \left[\cos kL - \frac{N-1}{N(kL)} \sin kL \right] \right|$$

$$\xi = A \frac{1}{\sqrt{S}} \cos(Kx - \phi)$$

$$\xi = \frac{A}{\sqrt{S_1(1-\alpha x)}} \cos(Kx - \phi)$$

$$\xi|_{x=0} = \xi_1$$

$$A = \xi_1 \frac{\sqrt{S_1}}{\cos\phi}$$

$$\xi = \frac{\xi_1}{\cos\phi(1-\alpha x)} \cos(kx - \phi)$$

$$\frac{\partial \xi}{\partial x} = \frac{\alpha}{(1-\alpha x)^2} \frac{\xi_1}{\cos\phi} \cos(kx - \phi) - \frac{\xi_1 k}{\cos\phi(1-\alpha x)} \sin(kx - \phi)$$

$$= \frac{\xi_1}{\cos\phi(1-\alpha x)} \left[\frac{\alpha}{1-\alpha x} \cos(kx - \phi) - k \sin(kx - \phi) \right]$$

$$\left. \frac{\partial \xi}{\partial x} \right|_{x=0} = 0$$

$$\tan\phi = -\frac{\alpha}{k}$$

$$X_M$$

$$\frac{\partial}{\partial x} \left(\frac{\partial \xi}{\partial x} \right) = 0 \Rightarrow \left[\frac{2\alpha^2}{(1-\alpha x)^3} - k^2 \right] \cos(kx - \phi) - \frac{2\alpha k}{(1-\alpha x)^2} \sin(kx - \phi) = 0$$

$$\tan(kx - \phi) = \frac{\alpha}{k} \frac{1}{1-\alpha x} - \frac{k}{2\alpha}(1-\alpha x)$$

$$\frac{k(\xi)_{max}}{\left(\frac{\partial \xi}{\partial x} \right)_{max}} = \varphi$$

$$\xi_{max} = \frac{\xi_1}{\cos\phi(1-\alpha L)} \cos(kL - \phi) = \frac{N\xi_1}{\cos\phi} \cos(kL - \phi)$$

$$\left(\frac{\partial \xi}{\partial x} \right)_{max} = \frac{\xi_1}{\cos\phi(1-\alpha x_M)} \left[\frac{\alpha}{1-\alpha x_M} \cos(k x_M - \phi) - k \sin(kx_M - \phi) \right]$$

$$\frac{\alpha}{k} \frac{1}{1-\alpha x_M} = \tan(kx_M - \phi) + \frac{k}{2\alpha}(1-\alpha x_M)$$

$$\left(\frac{\partial \xi}{\partial x} \right)_{max} = \frac{k\xi_1}{\cos\phi(1-\alpha x_M)} \left[\left[\tan(kx_M - \phi) + \frac{k}{2\alpha}(1-\alpha x_M) \right] \cos(k x_M - \phi) - \sin(kx_M - \phi) \right]$$

$$= \frac{\xi_1}{\cos\phi} \frac{k^2}{2\alpha} \cos(k x_M - \phi)$$

$$\varphi = \frac{k(\xi)_{max}}{\left(\frac{\partial \xi}{\partial x} \right)_{max}}$$

$$= \frac{kN\cos(kL - \phi)}{\frac{k^2}{2\alpha} \cos(k x_M - \phi)} = \frac{2\alpha N\cos(kL - \phi)}{k\cos(k x_M - \phi)}$$

Appendix B: MatLab Code for Plotting Analytical Calculations

Plot Code:

```
%Sample input
% E, Young's Modulus (MPa)
% RHO, Density (kg/m3)
% R1 Big-end Radius (mm)
% R2 Small-end Radius (mm)
% F, frequency (Hz)
% ZETA1, input displacement (mm)
R1=35;
R2=1;
E=210e3;
RHO=7900;
F=2.0e4;
ZETA1=1;
n=1;
i=1;
Mode =1;
;

[L,GAMMA,X0,XM,MP,PHI,PROF_UP,ZETAX,ZETADX,LABEL]=H_CON_HALF(E,RHO,R1,R2,F,ZETA1,n);
H_PLOT(L,X0,XM,PROF_UP,ZETAX,ZETADX,R1,R2,i,LABEL)
```

Calculation Code:

```
function
[L,ALPHA,X0,XM,MP,PHI,PROF_UP,ZETAX,ZETADX,LABEL]=H_CON_HALF(E,RHO,R1,R2,F,ZETA1,n)
% calculate parameters for catenary profile
% input
% E, Young's Modulus (MPa)
% RHO, Density (kg/m3)
% R1, Big-end Radius (mm)
% R2, Small-end Radius (mm)
% ZETA1, input displacement (mm)
% n, number of length
LABEL='Conical load free half wave length';
C=sqrt(E/RHO)*1e6;                  % Sound speed (mm/s)
N=R1/R2;                            % Radius ratio
K=2*pi*F/C;                         % wave number
% find K*L
myfun=@(KPL) tan(KPL)*(1+N*(KPL/(N-1))^2)-KPL;
KPL_N=fun_NsolveF(myfun,n,1,1,0.1,0);
L=KPL_N./K;
ALPHA=(R1-R2)./(R1.*L);
MP=abs(N*(cos(KPL_N)-(N-1)/(N*KPL_N)*sin(KPL_N)));
phi=atan2(-ALPHA,K);
% node and peak
```

```matlab
X0=-ones(n,n);
for i = 1:n
    for j=1:i
        X0(j,i)=(atan2(K,ALPHA(i))+(j-1)*pi)/K;  % Node position
(mm)
    end
end
XM=-ones(n,n);
for i = 1:n
    myfun2=@(XM_N)              tan(K*XM_N-phi(i))-ALPHA(i)/K*1/(1-
ALPHA(i)*XM_N)+K/(2*ALPHA(i))*(1-ALPHA(i)*XM_N);
    XM(1:i,i)=fun_NsolveF(myfun2,i,1,5,1e-2,1);
end
XMmax=diag(XM);
PHI=2.*ALPHA./K.*(N.*cos(K.*L-phi)./cos(K.*XMmax-phi));
syms x
% profile
PROF_UP=R1.*(1-ALPHA.*x);
% % displacement distributions
ZETAX=ZETA1./(cos(phi).*(1-ALPHA.*x)).*cos(K.*x-phi);
% % strain distributions
ZETADX=ZETA1./(cos(phi).*(1-ALPHA.*x)).*(ALPHA./(1-
ALPHA.*x).*cos(K.*x-phi)-K.*sin(K.*x-phi));
end
```

Appendix C: CNC G Code for Tool Path

```
( Rectangular Probing for Ultrasonic Sensor                    )
( This program repeatedly probes in a regular XY grid          )

(Configuration section)
G21    (G21 mm units G20 inches)
F50     (probe speed 5%)

#1= 0  (X start)
#2= 10 (X increment)
#3= 2 (X count)

#4= 0 (Y start)
#5= 1(Y increment)
#6= 40 (Y count)

#7= 0 (Z safety)
#8= -0.1 (Z probe)
(End configuration section)

#9=0 #10=0 (Counters)
G0Z#7
O1 while [#9 lt #6]
    #10=0
    G0 Y[#4+#5*#9]
    O2 while [#10 lt #3]
        O3 if [[#9/2] - fix[#9/2] eq 0]
            #11=[#1+#2*#10]
        O3 else
            #11=[#1+#2*[#3-#10-1]]
        O3 endif
        (#11 is X target)
        #5070=1
        O4 while [#5070 NE 0]
            G38.5 z#7
            G38.3 x#11
        O4 endwhile

        ( G38.2Z#8 Probing commented out)
        #10=[#10+1] (counter increment)
    O2 endwhile
    G0Z#7
    #9=[#9+1] (counter increment)
O1 endwhile

(G0X#1Y[#4+12])
M2 (program end)
```

Appendix D: Images of Veeco Optical Profiling Results
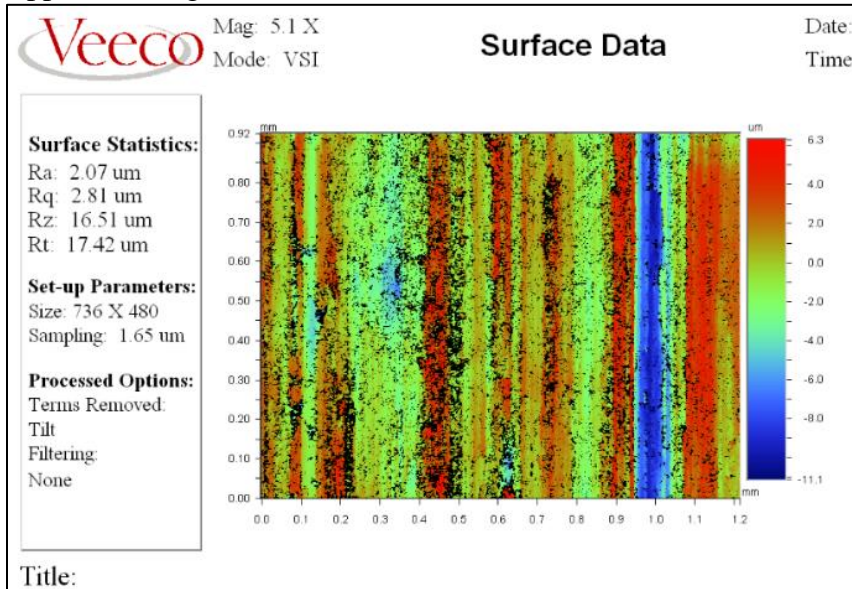
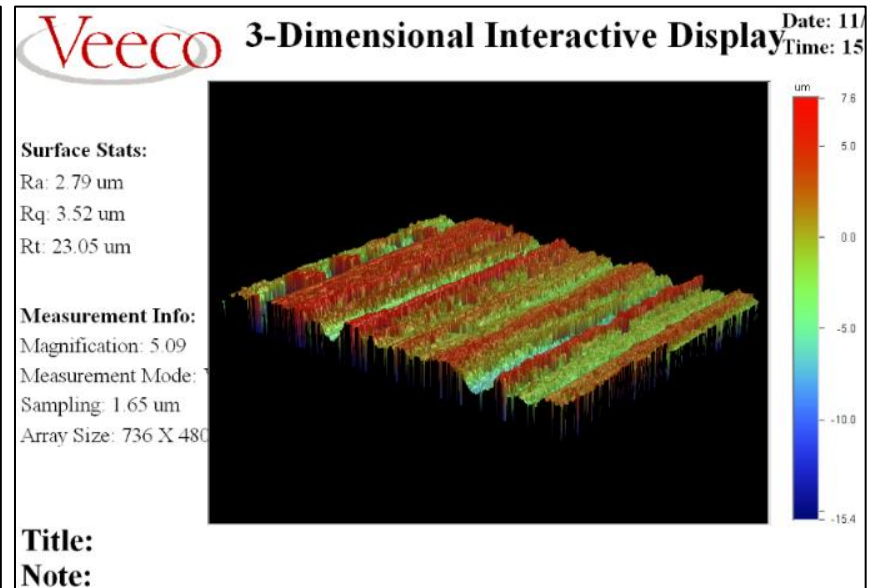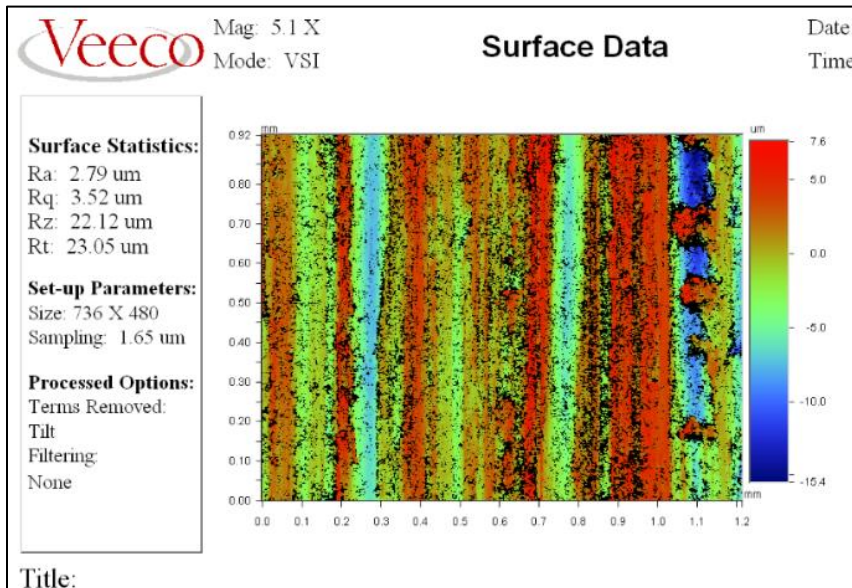Applied Voltage: 0V unprocessed
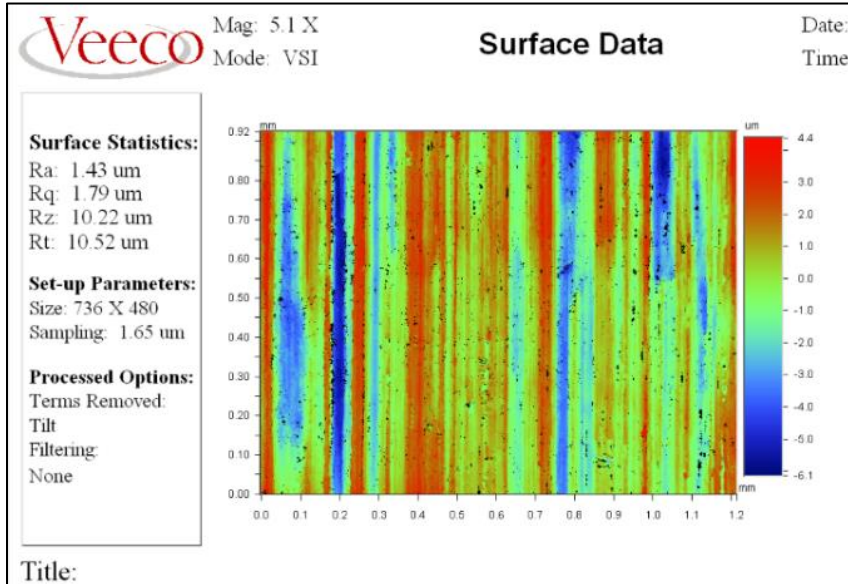
Zone A
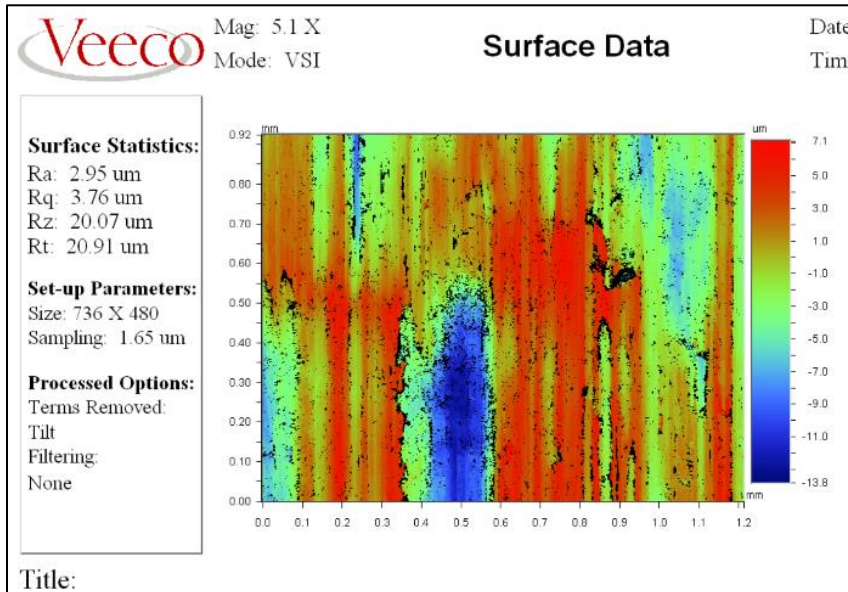
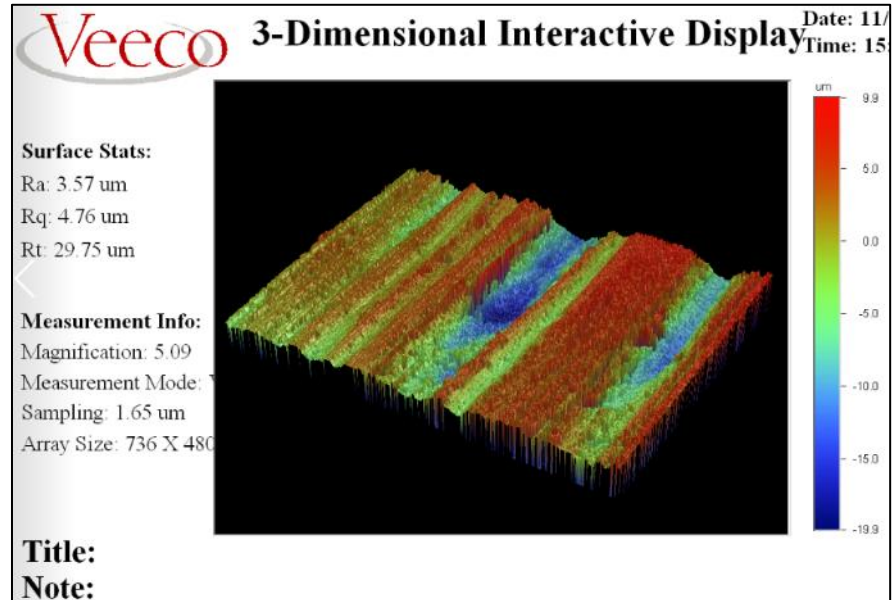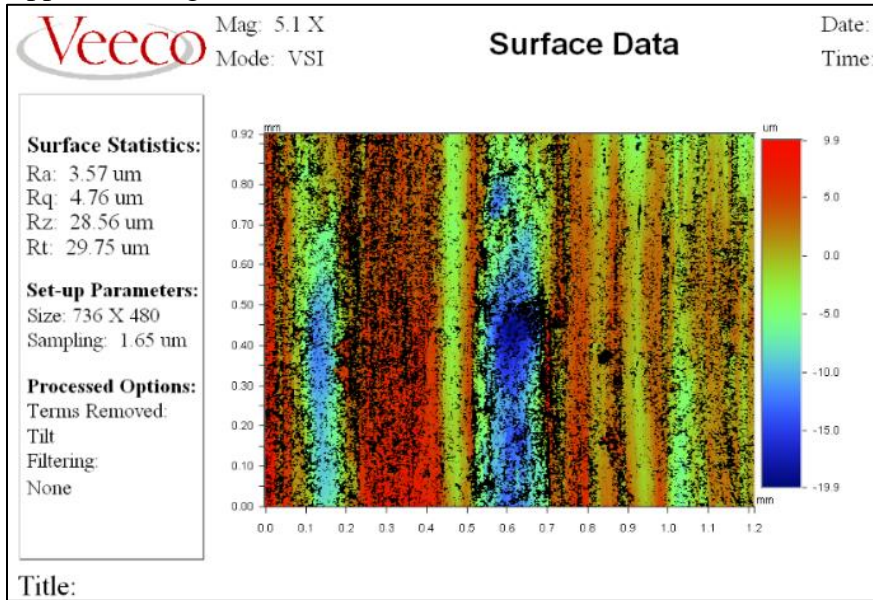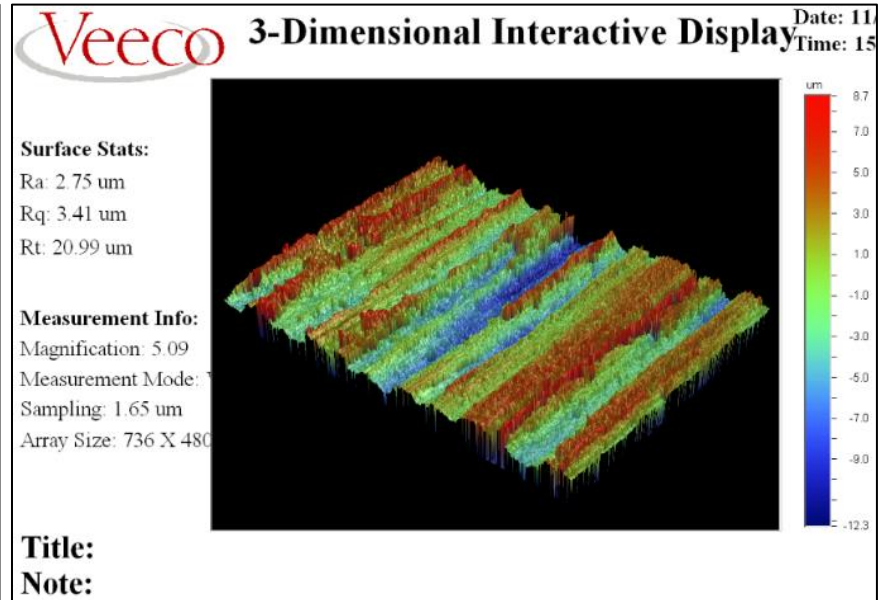

Zone B
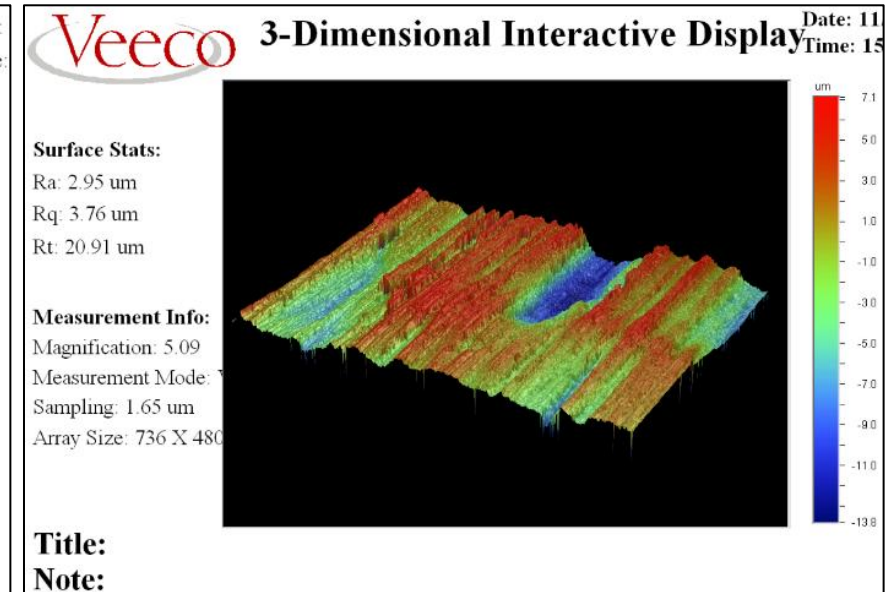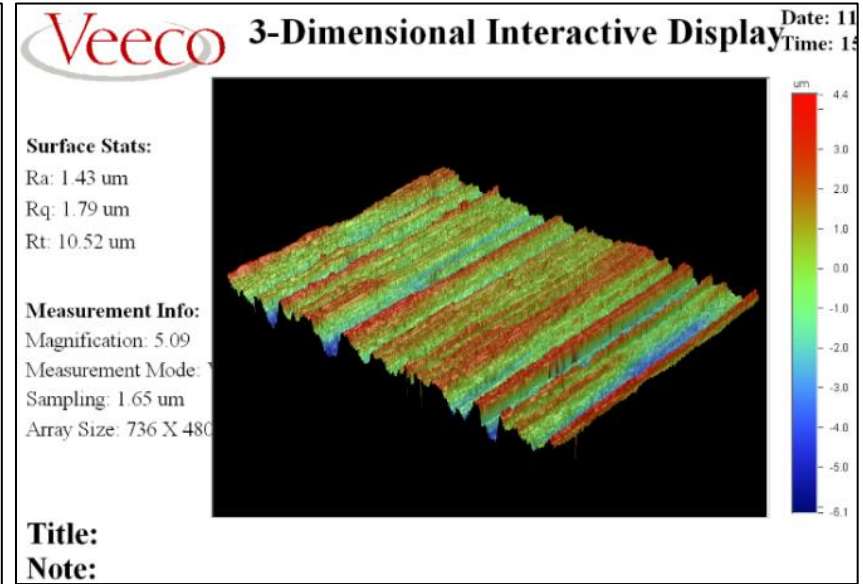
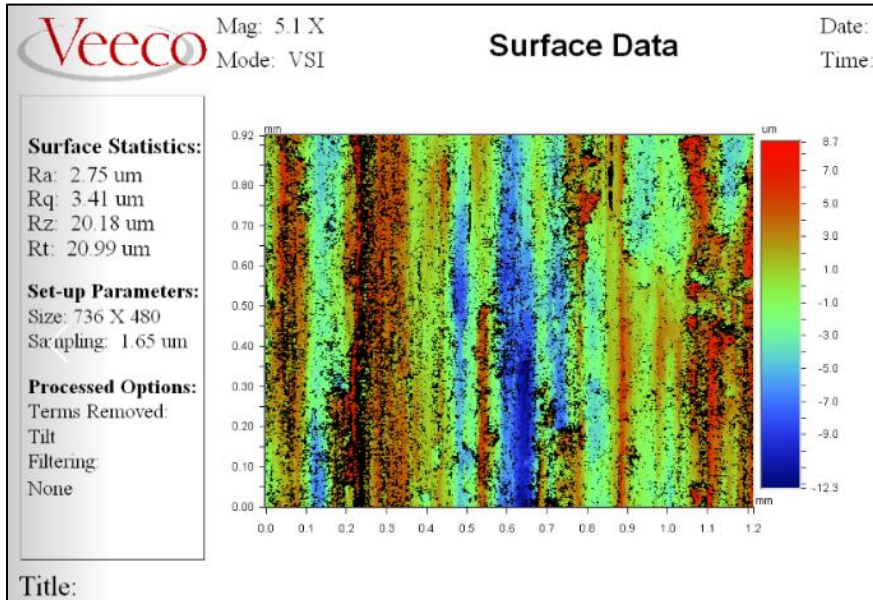Applied Voltage: 30V
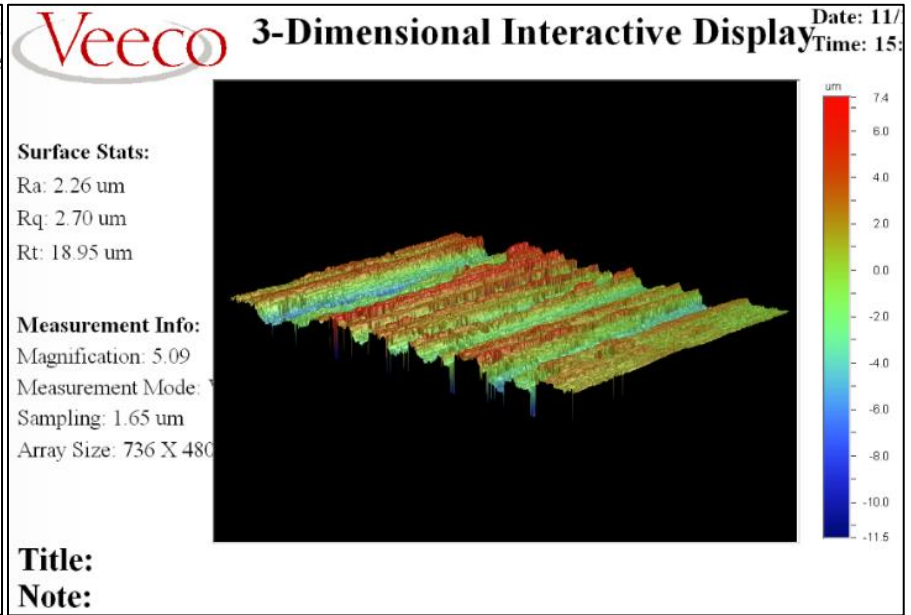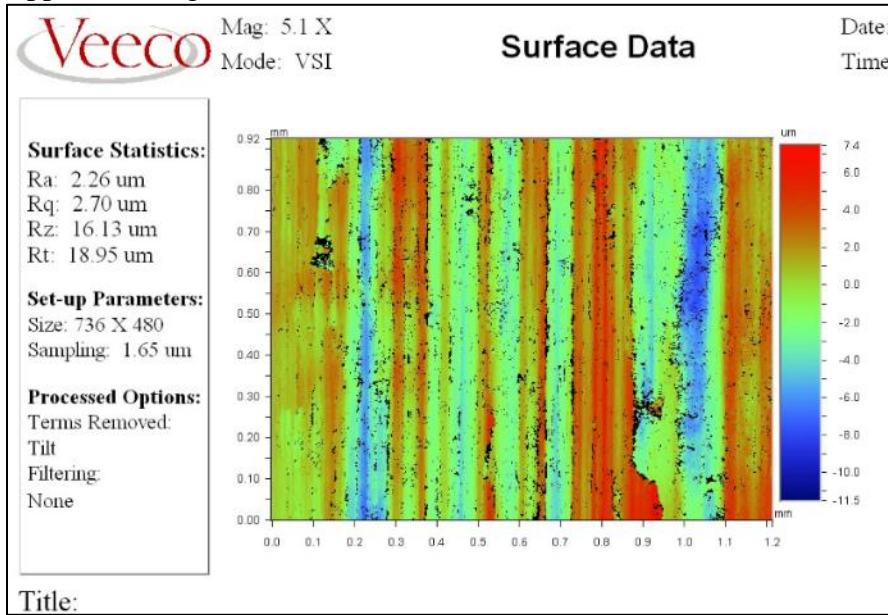
Zone A
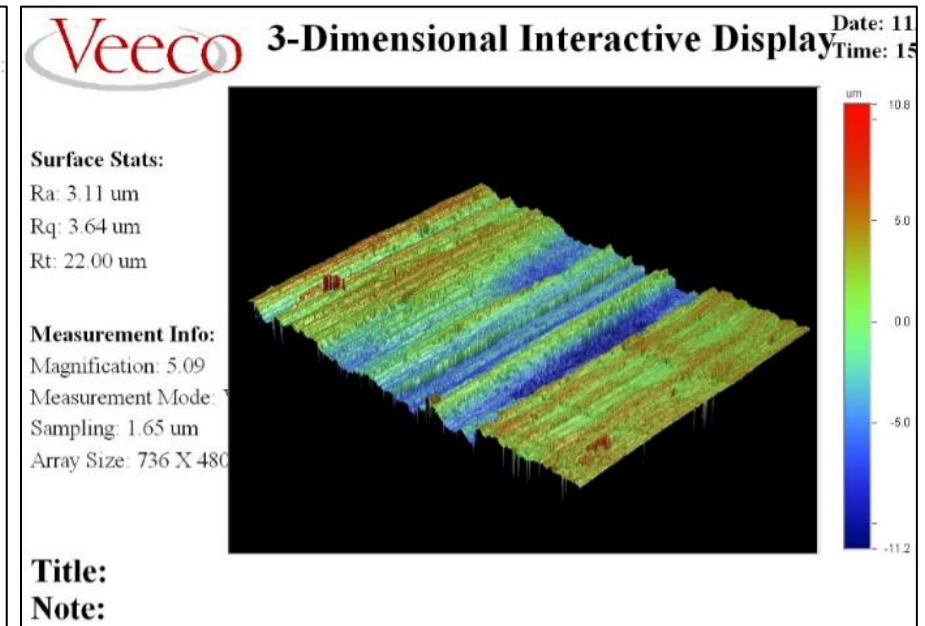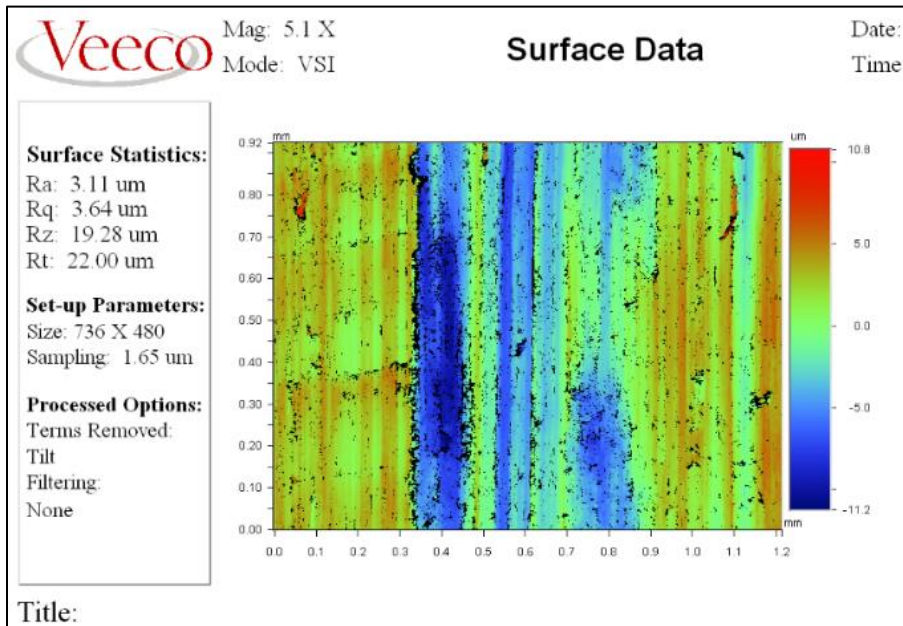
Zone B

Applied Voltage: 60V
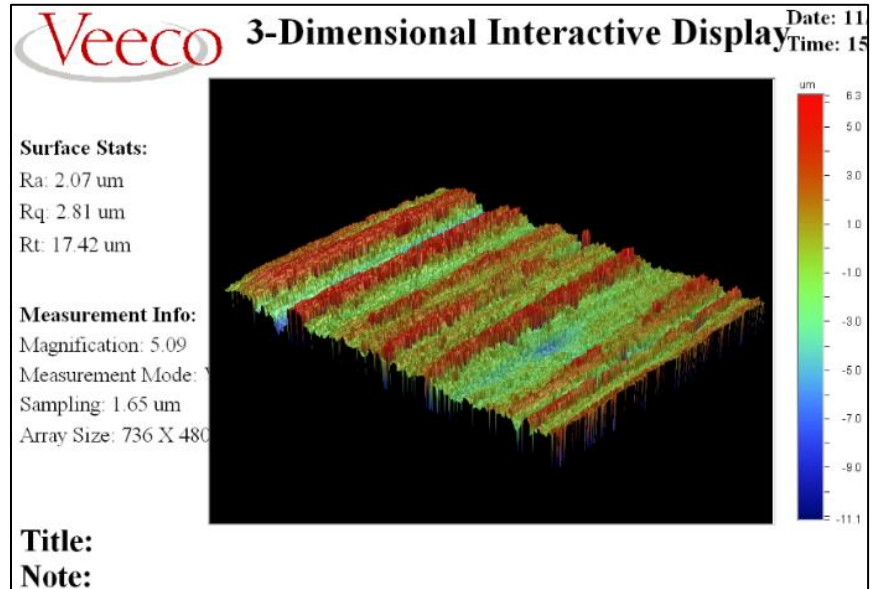
Zone A

Zone B

Applied Voltage: 90V

Zone A

Zone B